



Yann Rolland

Associate Professor at Université Savoie Mont Blanc. Laboratoire EDYTEM - UMR5204 Bâtiment « Pôle Montagne », 5 bd de la mer Caspienne, F-73376 Le Bourget du Lac cedex, France.

Tel : 0033-4 83 61 85 86, Yann.Rolland@univ-smb.fr

Antonin Bilau

PhD candidate at Edytem at Université Savoie Mont Blanc antonin.bilau@univ-smb.fr



Object: 20th November 2020

Article # se202-119 resubmission
to *Solid Earth*

To: *Solid Earth* Editorial Office
C. Sue editor

Dear editor(s),
Dear Christian Sue,

We are pleased to re-submit our manuscript entitled:

“Extensional reactivation of the Penninic Frontal Thrust 3 Ma ago as evidenced by U-Pb dating on calcite in fault zone cataclasite”,

authored by Antonin Bilau, Yann Rolland, Stéphane Schwartz, Nicolas Godeau, Abel Guihou, Pierre Deschamps, Benjamin Brigaud, Aurélie Noret, Thierry Dumont and Cécile Gautheron.

We are glad of the very positive and constructive reviews, and wish to thank the careful reading of the two reviewers. We followed most reviewer corrections, where possible, and in case of disagreement we explained why we kept our former interpretation. We also incorporated two new ages that comfort the previously obtained age of 3.5 Ma, as we obtained them after the submission process and they nicely confirm this age with a much narrower error bar.

We hope that you will find that the corrections have significantly improved the manuscript in a way to make it suitable for your journal.

Thanks also for the efficient editorial handling.

With kind regards, and on behalf of co-authors,

Antonin Bilau and Yann Rolland

Response to reviewer 1 (Alfons Berger):

General comments:

The paper gives constrain on the age of vein formation in(or near) the Penninic Frontal Thrust(=PFT). In addition,well performed stable isotopes of vein carbonates are used for reconstructing the fluid source of such veins. The data are all well performed and documented. The main problem may be a nomenclature problem. For many geologist, the name "PFT" is reserved for the thrusting of Pennine units on top of the foreland. This is not the topic of the paper. As you state in your abstract the vein formation and the extension is some how related "High-Durance Fault System"(see also your Line 97). In contrast, the introduction gives more an overview on the PFT, but not on the High-Durance Fault System. In other words, the introduction should give higher relevance to the Pliocene/Pleistocene extensional tectonics (e.g., Sue et al. 2007) instead on the Oligocene thrusting. The spatial overlap of the PFT and the High-Durance Fault should be described in detail at the beginning.

Thanks to Alfons Berger for his consideration and positive review. We reworked some sentences in order to precise the duality link between High-Durance Fault System and the PFT. However, here, we follow the common understanding of PFT in the western Alps, at the boundary with the Pelvoux Massif. Most authors argue that the HDFFS is the expression of the PFT reactivation as a normal structure in Briançonnais zone (following especially, Sue and Tricart, 1999, 2003). So, we don't think this might lead to some confusion between the two. To ensure a good comprehension of the meaning of the two systems PFT/ HDFFS, we made efforts to clarify this view as much as possible.

Detail comments :

Line 19:add "so called" or introduce somehow the "High Durance extensional fault"

OK. Modified.

Line 29/30:This sentence may be to complex for most readers.

"Extension is caused by compression, which is propagating..."???

OK, we modified the text for more clarity.

"This reactivation may result from the westward propagation of the compressional deformation toward the External Alps, combined to the exhumation of External Crystalline Massifs. In this context, the exhumation of the dated normal faults is linked to the eastward

translation of the HDFS seismogenic zone in agreement with the present day seismic activity."

Line 81: You may add "Agard et al. (2002)"
Read & Added.

Line 83: better see "Rubatto and Hermann (2001)"
Read & Added.

Line 90: The sentence is misleading. In Simon Labric et al. 2009 there is also whitemica from the PFT itself.
OK, corrected. We agree.

Line 96: see also constrains for the deformation history of the Briançonnais and Subbriançonnais in Ceriani and Schmid (2004) and related literature (Ceriani, Bucher etc).
Read & Added.

Line 113: please add a reference (or a figure).
Added, Fig.2.

Line 299: FT ages only record cooling, which require some how also erosion at the end. It is difficult to constrain the tectonics out of the FT data, specially if the ages are overlapping ages of both sides of the PFT.
We agree with you, FT ages are not direct datings of tectonic motions, and their signal can be misleading in this matter. However, as these were the only data that existed before to constrain PFT extensional motion, and as ages obtained on both sides of the PFT do not overlap there is a suggestion of PFT activity that is worth mentioning.

Response to reviewer 2:

Thanks a lot to Rev. 2 for his careful reading and advise about our paper. We followed his propositions in detail.

abstract

line 29-31: the discussion on the coeval extension in the internal zones and compression propagation in the external zone is not well constrained/dated and is not properly address in the discussion part of the ms. a specific paragraph could be added in the discussion. However, it is not a key point of the paper, and could be discarded.
OK. Reworked.

1. introduction

line 46: does the PFT really acted as a “plate boundary”? eventually discuss and/or present the structural relations between the Briançonnais and the external zone.

Right, modified : “as the major tectonic structure”.

line 48: also refer to Sue and Tricart (1999, Eclogae Geol. helv. ;2003, Tectonics) for the reactivation of the PFT in extension and the description of the regional fault system.

Read & Added.

line 51 also refer to Sternai et al. (2019, ESR) for the isostatic/buoyancy forces discussion.

Read & Added.

2. Geological setting.

line 64-67: the concept of “plate boundary” implies to consider the briançonnais zone as a single (micro)plate. I do think that this point deserves a longer analyze, specifically in terms of paoleogeography. Quote also Tricart, (1984, Am. J. Sci) for the PFT top-to-the-west thrusting history.

Right, modified : «as the major tectonic structure”.

line 68: Zhao et al (2016) is an important reference in the frame of this ms. but not on the nappe-related structure. Write a specific sentence for the lithospheric structure seen by Zhao et al.

Completed with « Schmid and Kissling 2000, Lardeaux et al., 2006, Malusà et al., 2017” . And Ceriani et al. for the nappe structure.

line 80-82: also quote Agard (2002 J. Metam. Geol).

Read & Added.

line 94-95: also quote the synthesis of Bertrand and Sue (2017, Swiss J. Geosci.)

Read & Added.

line 97-101: the overall seismotectonic local framework in the study area, including geodesy, should be better exposed. See for instance the recent paper by Mathey et al., (2020, GJI). the same matter arises in the discussion part.

Read & Added.

line 96: Note that the very first reports of the briançonnais’ seismicity has been published by Rothè (1941). The seismotectonic regional frame is

first described by Sue et al. (1999, JGR); these references could be added.

OK, very well. These refs have been added.

line101: the Jenatton et al (2007) and Leclère et al. (2012)'s works focused on the Ubaye swarm, to the South of the study area, which actually occurred West of the PFT, with fluid circulation. This thematic could be discussed in the ms., but in a specific paragraph, as these works are not directly connected to the PFT reactivation.

Right, removed.

line 120: the same Oreac section has been described by Sue and Tricart (1999, Eclogae Geol. Helv.) in term of brittle deformation and related paleostress.

Read & Added.

3. Sampling strategy and analytical method

this part is well organized, precise and informative.

Fine. Thank you.

4. Results

fig4a: could you provide the corresponding photography? give also a close-up location map of the samples (smaller scale than fig.2).

Modified, the original photography is in Fig.3c.

line 243 and following: better explain the stable isotope results, for a non-specialist.

Addition of formulation of equation (1): $\delta^{13}C$ calculation. And "The ratio of carbon and oxygen isotopes is related to the parental fluid of calcite and can be used as a fluid tracer."

line 262-263: the comparison with the Mont-Blanc ECM is very interesting. It must be better developed in the discussion part. In the present form, the last sentence of the paragraph is unuseful. Either discard it, or (better) develop a bit more.

OK, discussion and links with the Mt-Blc have been developed.

line 275-276: better explain this sentence (re-write).

Reworked and completed. The details pertaining to analytical proc. have been better explained in the corresponding section.

line 277-283: these ages are very good regarding the questions still under debate on the overall late extension thematic. Moreover, they

represent the core of the paper. I would advise to better underline the quality and novelty of these pretty young ages.

Thanks for this comment. We complemented this section and reworked the conclusion to highlight those ages and corresponding fluid history better.

Fig7 could be enlarged. The figures and words embedded in the panels are not legible.

OK, this has been done. In addition, 2 more ages coming from new sample in the same area have been added, and elemental map see supplementary data.

5. Discussion

the overall discussion is written with a pretty affirmative tone. I suggest the authors to use more careful words in their interpretations.

Taken into account, sentences have been rewritten in a less affirmative way.

line 319-320: precise and rewrite the 3 points (i) (ii) and (iii) in a more logical way.

Reworked and completed: « (i) lack of large-scale structures (ii) pressure-solution microstructures (evidence of local fluid) (iii) presence of a shallow impermeable clay layer which isolate surface and deep systems”.

line 332-333: this sentence is unclear. rewrite and develop a bit the concept you wanna describe.

OK, rewritten.

line 340-345: the comparison with the Mont-Blanc ECM deserves to be better developed. I would suggest to write a complete paragraph on this comparison, eventually supported by a new specific figure, including a map view of the related MB vs. Brian-connaix contexts. Concerning the MB's exhumation processes, quote at least Seward and Mancktelow (1994, Geology).

This comparison has been precised, with some more details on the MB context. However, besides this is clear that fluids have a similar signature, the age of structures is different (15 Ma in Mt Blc) and so is the context (extensional here, compressional Mt Blc), so we don't think the comparison has to be so much extended.

Line 347, together with Zhao et al (2016), the references to the ECORS profile and related interpretations regarding the PFT at depth must be quoted (e.g. Mugnier et al., BSGF 1993). I also suggest to quote the

ECORS cross-section re-assessed by Schmid and Kissling (2000, Tectonics).

OK, these refs have been added.

line 380: the fault dated in the ms. “may” represent a paleo-HD fault. It is still an interpretation.

Added.

line389-400: this very small paragraph on “evolution through time” (indeed from c.a. 3 Ma up to now and the active deformation) must be better developed and improved. A map of the active deformation at the local scale could be interesting. The paragraph should integrate discussion on the uplift, which is not restricted to the ECM, but also affect the inner area (Nocquet et al. 2016; Sternai et al., 2019), together with the extension seen both in geodesy (e.g. Walpersdorf et al., 2015, J. Geodyn) and looking at the focal mechanisms of earthquakes (Sue et al. 1999 JGR ; 2007 IJES). Indeed, such a discussion should bring the gap between the current activity of the Briançonnais area, which is well constrained, and the “late alpine” faulting, which is now well dated by the present paper.

OK, we agree, we have enhanced this part.

Response to Topical Editor:

Both reviewers agreed since the first run of revision that the manuscript is an interesting contribution suitable to be published in the SE Special issue. I’m completely in agreement with the reviewers especially now that the manuscript is also improved taking into account the suggestions and comments of both reviewers.

I recommend therefore acceptance of this very nice paper maybe considering some changes included in the annotated pdf (text and one figure).

I suggest to change the "stress-related" term of "compression" with "contraction or shortening" if as in your case is used in combination with extension (indeed a "strain -related" term).

Note however that the Figure 9 stage "present day" compression is written with only 1 s. compression please change

Thanks, the manuscript has been corrected accordingly to the consideration for the use of the term "shortening" instead of "compression".

1 **Extensional reactivation of the Penninic Frontal Thrust 3 Ma ago as** 2 **evidenced by U-Pb dating on calcite in fault zone cataclasite.**

3
4 Antonin Bilau^{a,b}, Yann Rolland^{a,b}, Stéphane Schwartz^b, Nicolas Godeau^c, Abel Guihou^c, Pierre
5 Deschamps^c, Benjamin Brigaud^d, Aurélie Noret^d, Thierry Dumont^b, and Cécile Gautheron^d.

6 ^aEDYTEM, Université Savoie Mont Blanc, CNRS, UMR 5204, Le Bourget du Lac, France.

7 ^bISTerre, Université Grenoble Alpes, Univ. Savoie Mont Blanc, CNRS, IRD, IFSTTAR, 38000
8 Grenoble, France.

9 ^cAix-Marseille Université, CNRS, IRD, INRAE, Collège de France, CEREGE, Aix en Provence,
10 France.

11 ^dGEOPS, CNRS, Université Paris-Saclay, 91405 Orsay, France.

12 **Correspondence:** Antonin Bilau (antonin.bilau@univ-smb.fr) and Yann Rolland
13 (Yann.Rolland@univ-smb.fr).

14 **Abstract**

15
16 In the Western Alps, the Penninic Frontal Thrust (PFT) is the main crustal-scale tectonic structure of the
17 belt. This thrust transported the high-pressure metamorphosed internal units over the un-metamorphosed
18 European margin during the Oligocene (34-29 Ma). Following the propagation of the compression
19 toward the European foreland, the PFT was later reactivated as an extensional detachment associated
20 with the development of the High-Durance extensional fault system (HDFS). This inversion of tectonic
21 displacement along a major tectonic structure has been widely emphasized as an example of extensional
22 collapse of a thickened collisional orogen. However, the inception age of the extensional inversion
23 remains unconstrained. Here, for the first time, we provide chronological constraints on the extensional
24 motion of an exhumed zone of the PFT by applying U-Pb dating on secondary calcites from a fault zone
25 cataclasite. The calcite cement/veins of the cataclasite, formed after the main fault slip event, at 3.6 ± 0.4 -
26 3.4 ± 0.6 Ma. Cross-cutting calcite veins featuring the last fault activity are dated at 2.6 ± 0.3 - 2.3 ± 0.3 Ma.
27 $\delta^{13}\text{C}$ and $\delta^{18}\text{O}$ fluid signatures derived from these secondary calcites suggest fluid percolation from deep-
28 seated reservoir at the scale of the Western Alps. Our data evidence that the PFT extensional reactivation
29 initiated at least ~ 3.5 Ma ago with a reactivation phase at ~ 2.5 Ma. This reactivation may result from
30 the westward propagation of the compressional deformation toward the External Alps, combined to the
31 exhumation of External Crystalline Massifs. In this context, the exhumation of the dated normal faults
32 is linked to the eastward translation of the HDFS seismogenic zone in agreement with the present day
33 seismic activity.

34 **1. Introduction**

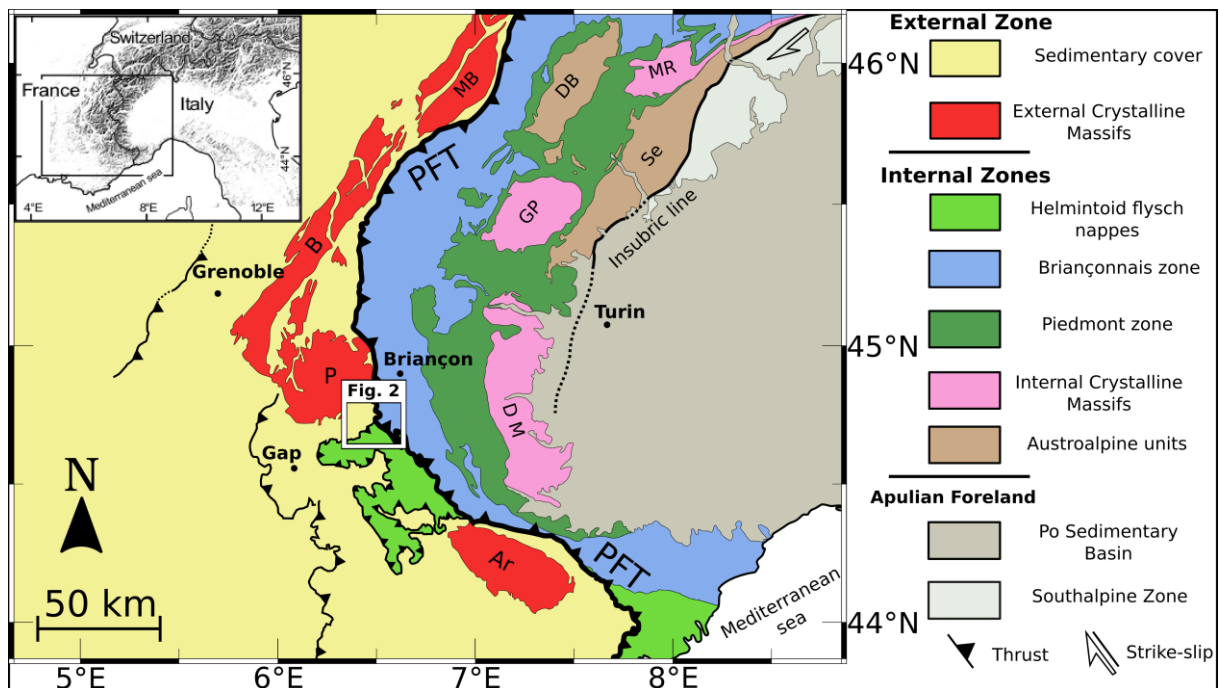
35 Dating of major tectonic inversions in orogens is generally achieved by indirect and relative dating, but
36 rarely by the direct dating of fault-related minerals using absolute geochronometers. For instance,
37 tectonic cycles are defined worldwide by the sediment unconformities or by exhumation ages through
38 thermochronological investigation. However, the recent progress in U-Pb dating of carbonate using
39 high-resolution Laser Ablation analyses (Roberts et al., 2020) allows us to directly date minerals formed
40 during fault activity and thus to establish the age of tectonic phases by absolute radiometric dates (Ring
41 and Gerdes, 2016; Goodfellow et al., 2017; Beaudoin et al., 2018;). This method is especially well suited
42 to disentangle the successive tectonic motions along a given tectonic structure. U-Pb dating can be
43 coupled to stable isotopic analysis to infer the nature of fluids through time, which may give insights of
44 the scale of fluid circulations and thus the scale of the active tectonic structure and changes in the stress
45 regime (e.g., Beaudoin et al., 2015; Rossi and Rolland, 2014). In the Western Alps, the Penninic Frontal
46 Thrust or PFT represents a major thrust structure at lithospheric scale (e.g., Tardy et al., 1990; Mugnier
47 et al., 1993; Zhao et al., 2015) that accommodated the main collisional phase during the Paleogene-
48 Neogene (e.g., Ceriani et al., 2001; 2004). Later on, this thrust was reactivated as a normal fault, and the
49 extensional deformation is still ongoing (Sue and Tricart, 1999; Tricart et al., 2006; Sue et al., 2007).
50 This transition from compression to extension in a collisional chain has been diversely interpreted to
51 reflect slab breakoff, crustal overcompensation or post-glacial and erosion-induced isostatic rebound
52 (e.g., Champagnac et al., 2007; Sternai et al., 2019). However, until now, no direct dating of the tectonic
53 shift from compression to extension on the PFT has been obtained, which leads to many possible
54 geodynamic scenari. At the present day, a large range of ages for this transition has been hypothesized
55 from ~12 to 5 Ma (Tricart et al., 2006), to only few ten's ka (Larroque et al., 2009) which shows the
56 lack of direct dating of brittle deformation (Bertrand and Sue, 2017). In this study, we applied the Laser
57 Ablation U-Pb dating method on secondary calcites from a cataclasite fault zone that testify of the
58 extensional deformation of an exhumed paleo-normal fault during the PFT inversion.

59 The purpose of this study is (1) to provide absolute chronological constraints on the structural inversion
60 of the PFT, and (2) give insights into the scale and nature of fluid circulations along this major fault
61 using stable isotope analysis of carbon and oxygen.

63 **2. Geological setting**

64 The western Alpine collisional belt results from the convergence and collision of the European and
65 Apulian plates, which culminated with top-to-the west displacement on the PFT acting as the major
66 Alpine tectonic structure in the Late Eocene to Oligocene times (e.g., Dumont et al., 2012; Bellahsen et
67 al., 2014). This lithospheric-scale structure accommodated westward thrusting of highly metamorphosed
68 "Internal zone" units over slightly metamorphosed "External zone" units (Fig. 1, Schmid and Kissling

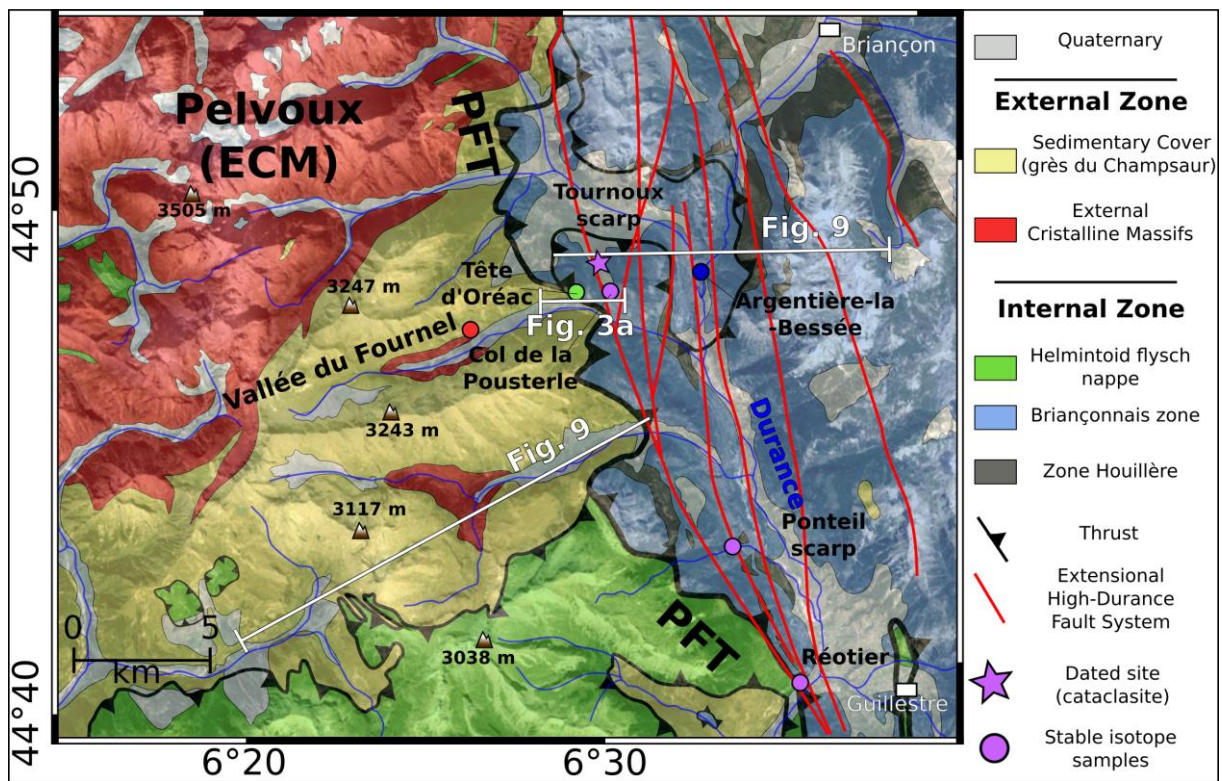
69 2000; Lardeaux et al., 2006; Simon-Labric et al., 2009; Malusà et al., 2017). The External zone is
 70 composed of the European non-metamorphosed Mesozoic and Paleozoic sedimentary cover and its
 71 Paleozoic basement corresponding to the External Crystalline Massifs.



72
 73 **Fig. 1.** Geological map of Western Alps showing the location of the study area. External Crystalline Massifs: Ar,
 74 Argentera; B, Belledonne; MB, Mont Blanc; P, Pelvoux. Internal Crystalline Massifs: DM, Dora-Maira; GP,
 75 Grand Paradis; MR, Mont Rose. PFT: Penninic Frontal Thrust. Insert modified from Schwartz et al. (2017).

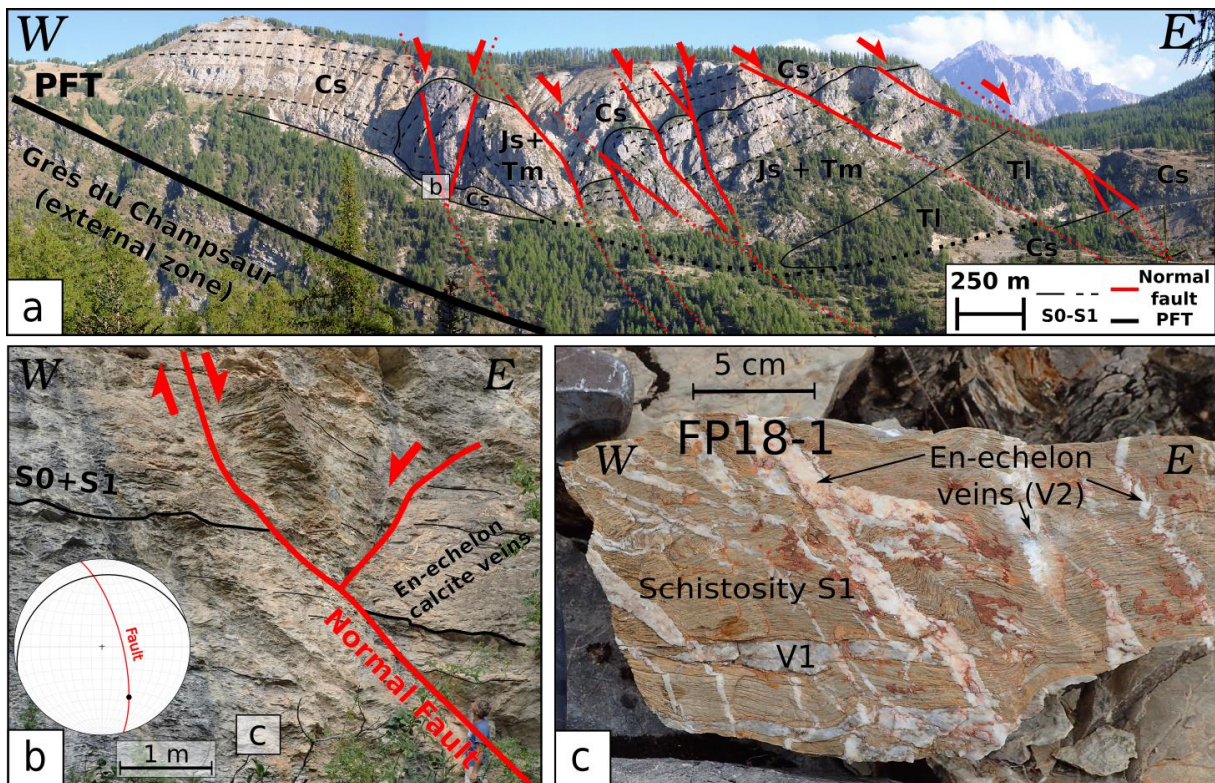
76
 77 The Internal zone corresponds to a high-pressure metamorphic wedge formed by the stacking of the
 78 paleo-distal European margin of the Briançonnais zone, comprising the Internal Crystalline Massifs and
 79 their sedimentary cover, with the oceanic-derived units of the Piedmont zone. These units were
 80 incorporated and juxtaposed in the subduction accretionary prism since the Early Late Cretaceous until
 81 the Late Eocene (e.g., Agard et al., 2002; Schwartz et al., 2007). The timing of subduction and collision
 82 is well constrained by numerous dates on metamorphic minerals (e.g., Duchêne et al., 1997; Rubatto
 83 and Hermann, 2001; Lanari et al., 2012, 2014). Eclogite facies recrystallization records subduction of
 84 the distal European margin at 32.8 ± 1.2 Ma in the Dora Maira massif, which was later transported as a
 85 tectonic nappe during the collision (Duchêne et al., 1997). PFT activation and underthrusting of External
 86 Crystalline Massifs are indicators of the transition from subduction to continental collision in the Internal
 87 zones, between 44 and 36 Ma (e.g., Beltrando et al., 2009). This transition is marked by shear zone
 88 development at greenschist facies conditions and recrystallization during burial of the Alpine External
 89 zone in the PFT footwall compartment (Rossi et al., 2005; Sanchez et al., 2011; Bellahsen et al., 2014).
 90 The early ductile PFT activity is dated at 34-29 Ma by $^{40}\text{Ar}/^{39}\text{Ar}$ dating of syn-kinematic phengite from
 91 shear zones in the Pelvoux and Mont Blanc External Crystalline Massifs (Seward and Mancktelow,

1994; Rolland et al., 2008; Simon-Labric et al., 2009; Bellanger et al., 2014; Bertrand and Sue, 2017) and by U-Pb on allanite (Cenki-Tok et al., 2014). The age of the PFT hanging wall tectonic motion and joint erosion is highlighted by the exhumation of the Briançonnais units constrained by apatite fission tracks (AFT) at 26-24 Ma (Tricart et al., 1984, 2001, 2007; Ceriani and Schmid, 2004). However, the PFT reactivation as a normal fault remains unconstrained. The onset of PFT extensional activity has been proposed to the Late Miocene (~12 to 5 Ma), based on indirect AFT ages in the Pelvoux External Crystalline Massif (Tricart et al., 2001, 2007), that record a cooling episode related to relief creation and erosion. The current seismicity (e.g., Rothé, 1941; Sue et al., 1999, 2007) and observed GPS motions (Walpersdorf et al., 2018; Mathey et al., 2020), all along the so-called High-Durance Fault System (HDFS) highlight the fact that extensional and minor strike-slip deformations along the PFT are still ongoing. This seismicity mostly occurs at shallow depths, less than 10 km, and mainly at 3 to 8 km, where the HDFS is structurally connected to the PFT (Sue and Tricart 2003, Thouvenot and Fréchet, 2006; Sue et al., 2007).



105 **Fig. 2.** Study area of the Penninic Frontal Thrust, east of the Pelvoux External Crystalline Massif (ECM). High-
 106 Durance Fault System is represented in red from Tricart et al. (2001) and Sue et al. (2007). Location of sampled
 107 sites is indicated. The location of the extensional fault dated by U-Pb on calcite (samples FP18-2 and FP18-3)
 108 is marked by a star. Colour of site circle refers to the host rock age: red, Eocene sandstone flysch (grès du
 109 Champsaur); green, Cretaceous carbonates; blue, Jurassic carbonates; purple, Triassic carbonates. Sample
 110 descriptions are shown on Suppl. Mat. 1. © Google Earth for background relief map.

111 The study area is focused on a portion of the PFT located in the southeast of the Pelvoux External
 112 Crystalline Massif in the Western Alps (France) (Figs. 1-2). Here, the PFT rests on Late Eocene
 113 (Priabonian) autochthonous nummulitic flysch so-called the “Champsaur sandstone” (Fig. 2), which lies
 114 unconformably on the Pelvoux crystalline basement. In the southern part, the PFT lies on the Cretaceous
 115 Helmintoid flysch nappes, Fig. 2. These two flysch units are intensely deformed by top-to-the-west PFT
 116 compressional deformation. The PFT hanging wall corresponds to the Briançonnais zone composed of
 117 Mesozoic and Paleozoic sedimentary units, which underwent high pressure metamorphism (Lanari et
 118 al., 2012; 2014). The Briançonnais zone is composed of the Briançonnais Zone Houillère, which consists
 119 of Carboniferous sediments overlying a crystalline basement, stratigraphically overlain by Middle
 120 Triassic to Cretaceous sediments (limestones and calcschists). The PFT structure is well shown in the
 121 Tête d’Oréac section of the Fournel Valley transect (Fig. 3, Sue and Tricart, 1999). Here, normal faults
 122 cross-cut the Briançonnais series and branch down on the PFT, which was reactivated as a detachment
 123 (Tricart et al., 2001).



124 **Fig. 3. a:** General view and geological interpretation of the Fournel Valley southern slope with the studied site of
 125 the Tête d’Oréac. **b:** Outcrop interpretation of the Tête d’Oréac with extensional features in late Cretaceous
 126 calcschists in agreement with the High-Durance Fault System and Wulff stereogram, lower hemisphere. **c:**
 127 Calcschist oriented sample FP18-1 evidencing multiple calcite vein generations. V1 is related to the main
 128 compressional phase related to the Tête d’Oréac anticline formation and V2 are related to extensional reactivation
 129 of the PFT during onset of the High-Durance Fault System. Cs: Late Cretaceous calcschists; Js+Tm: Middle
 130 Triassic to Late Jurassic dolomitic to siliceous limestones; Tl: Lower Triassic sandstones.

131 The normal faults are tilted by a passive rotation of about 30 degrees towards the west during their
132 exhumation in relation with the activity of the High-Durance Fault System (Sue et al., 2007).

133

134 **3. Sampling strategy and analytical methods**

135 *3.1. Sampling strategy*

136 We collected key samples of each brittle-ductile deformation phase, both in the PFT footwall and
137 hanging wall (Suppl. Mat. 1), to provide a petrographic and stable isotopic dataset which will allow
138 discussing the nature of fluids throughout the PFT activity associated to the late compressional and
139 extensional history. Field analysis is supported by petrographic observations on 28 samples, including
140 8 host rocks, 6 from compressional structures and 14 from **extensional** structures. Based on this dataset,
141 we selected three fault breccia samples to date the PFT extensional reactivation.

142

143 *3.2. Cathodoluminescence*

144 Cathodoluminescence (CL) analysis provides shades that are mainly representative of oxidation state of
145 trace element and their contents, i.e. Mn^{2+} and Fe^{2+} (Barnaby and Rimstidt, 1989). These differences in
146 calcite chemical composition are an indicator of different mineral precipitations related to slight
147 variations in fluid composition (Goodfellow et al., 2017). CL can also highlight crystal growth patterns
148 or grain boundary interactions (Beaudoin et al., 2015). Using cross-cutting criteria as well as CL, a
149 relative chronology of the calcite generations and related microstructures has been made. Analyses were
150 performed with a spot camera mounted-Cathodyne device (cold cathode) with the following parameters:
151 vacuum ~50mTorr; voltage 16-18 kv; electron beam ~200 μA . Used description terminology is based
152 on Bons et al. (2012).

153

154 *3.3. O and C stable isotope analysis*

155 Stable isotope measurements were achieved on the different generations of microstructures identified
156 by thin section observations and CL images, at Geosciences Paris Sud (GEOPS) laboratory of the Paris-
157 Saclay University, France. Results are presented in Table 1. The protocol is described in detail by
158 Andrieu et al. (2015). Several milligrams (~1mm³) of sample for each calcite generation were collected
159 using a Dremel 4000 with a 3.2 mm head. Samples were then dissolved with pure orthophosphoric acid
160 (H_3PO_4): Sample tubes provided with two compartments (one for the sample and one for the acid) were
161 sealed under a pressure of 1.5×10^{-2} mbar. They were immersed in a water bath at 25°C before the acid
162 was poured on the sample and let to react for 24 h. Complete reaction is necessary to avoid any artificial
163 isotopic fractionation. The produced CO_2 is collected using an extraction line and a liquid nitrogen trap
164 is used to ensure that only CO_2 is collected. Pure CO_2 is analyzed on a VG Sira 10 dual inlet IRMS
165 (Isotope Ratio Mass Spectrometer). Data validity is supported by concurrent analysis of the international

166 standard IAEA CO-1. $\delta^{13}\text{C}$ and $\delta^{18}\text{O}$ are expressed in ‰ relative to V-PDB (Vienna Pee Dee Belemnite)
167 by assigning a $\delta^{13}\text{C}$ value of +1.95‰ and a $\delta^{18}\text{O}$ value of -2.20‰ to NBS19, (1).

$$168 \quad \delta^{13}\text{C} = \left[\frac{(^{13}\text{C}/^{12}\text{C})_{\text{Sample}}}{(^{13}\text{C}/^{12}\text{C})_{\text{Reference}}} - 1 \right] \times 1000 \quad (1).$$

169 For oxygen isotope measurements, switch from PDB values to SMOW (Standard Mean Oceanic Water)
170 were made using the Kim et al. (2015) equation, (2).

$$171 \quad \delta^{18}\text{O}_{\text{SMOW}} = 1.03086 \times \delta^{18}\text{O}_{\text{PDB}} + 30.86 \quad (2).$$

172 The ratio of carbon and oxygen isotopes is related to the parental fluid of calcite and can be used as a
173 fluid tracer. Reproducibility was checked by replicate analysis of in-house standards and was $\pm 0.2\%$ for
174 oxygen isotopes and $\pm 0.1\%$ for carbon isotopes.

175

176 *3.4. U-Pb dating of calcite*

177 In-situ uranium and lead isotope analyses of carbonates were carried out at CEREGE (Centre Européen
178 de Recherche et d'Enseignement des Géosciences de l'Environnement), Aix-en-Provence, France.
179 Results are presented in Suppl. Mat. 2. Data were acquired on 150 μm thick thin sections. Laser ablation
180 analysis was performed with an ESI excimer Laser Ablation system with a 6 inches two volume cell
181 (ESI), coupled to an Element XR SF-ICP-MS (Sector Field Inductively Coupled Mass Spectrometer,
182 Thermo-Scientific). Analyses were done at 10 Hz and 1.1-1.15 $\text{J}\cdot\text{cm}^{-2}$. Samples were first screened to
183 check signal intensities and maximise the spread of $^{238}\text{U}/^{206}\text{Pb}$ ratios (e.g. map of Suppl. Mat. 3) to obtain
184 the highest U-Pb variability. A typical analysis consists of 3 seconds of pre-ablation to clean the sample
185 surface, followed by 20 seconds of gas blank and ~ 20 seconds of measurement on a static circle spot of
186 150 μm diameter (approximately 8-9 acquisition cycles per second). These parameters lead to
187 approximately ~ 20 -25 μm depth hole (~ 1 $\mu\text{m}/\text{s}$) on a carbonate material. Ablated particles are carried
188 out of the cell with a He gas flux of 1300 ml/min and then mixed with Ar sample gas (typically 0.8-0.9
189 l/min). Unknown samples were corrected by standard bracketing with synthetic NIST-614 glass for
190 instrumental drift and lead isotope composition (Woodhead et al. 2001) and a natural calcite spar WC-
191 1 of 254.4 ± 6.4 Ma (Roberts et al., 2020) for inter-elemental fractionation effect, every 20
192 measurements. No downhole correction was applied since no natural calcite standard with homogeneous
193 U-Pb ratio allows such correction. However, the large aspect ratio used in this set up is supposed to limit
194 this effect. Unknown sample were first processed with the Iolite software (Paton et al., 2011) for baseline
195 correction. Raw ratios were then reduced for instrumental drift, lead isotope composition and inter-
196 elemental fractionation using an in-house excel spreadsheet macro designed for carbonate samples. Ages
197 are obtained using IsoplotR software and plotted in a Tera-Wasserburg diagram using model (1) age
198 (Vermeesch, 2018). An additional error propagation of 2.51% in quadratic addition on the final age, tied
199 to the WC-1 standard, is expressed in brackets in the Tera-Wasserburg plot.

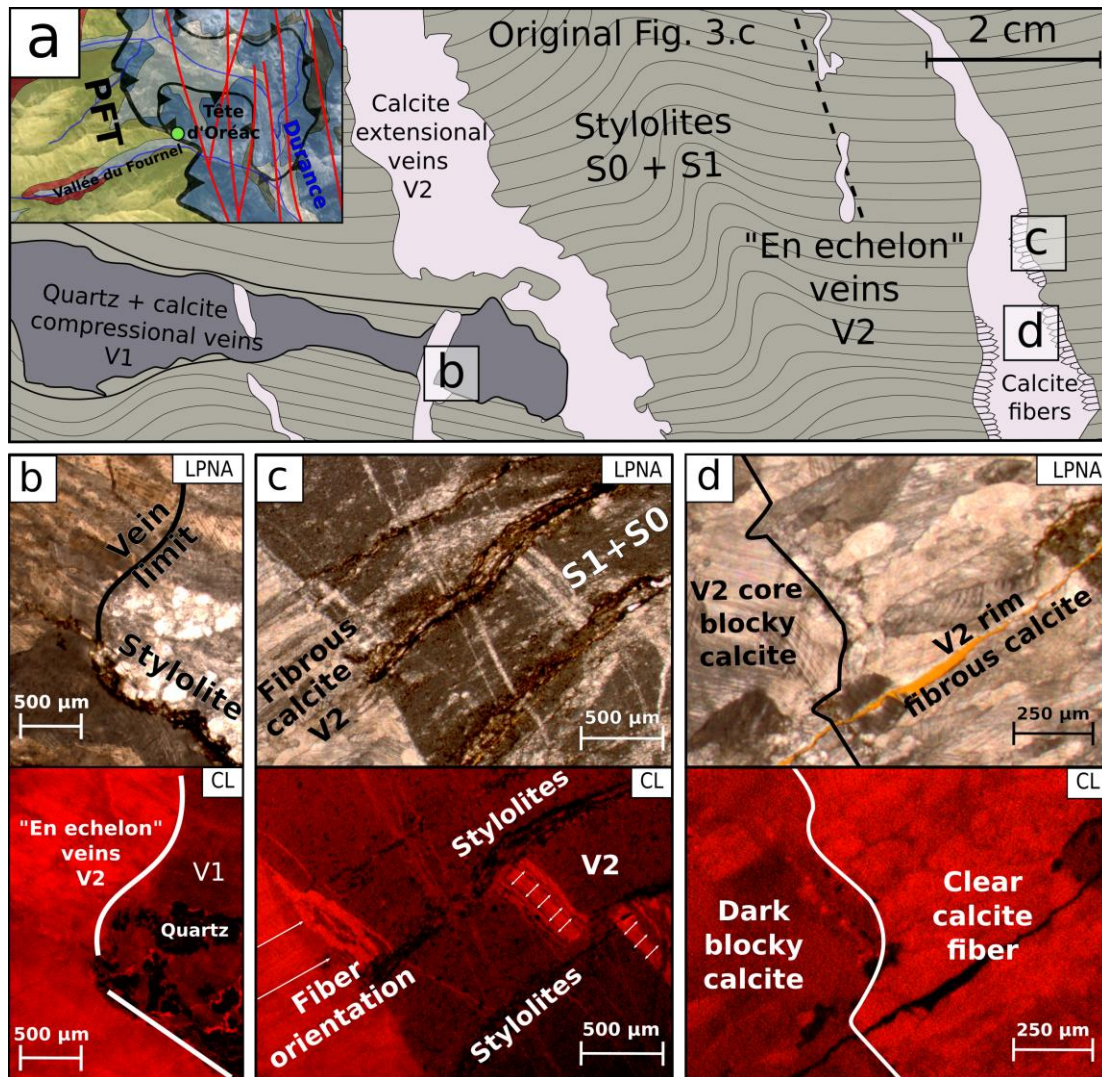
200
201
202
203
204
205
206
207
208

4. Results

4.1. Deformation phases and microstructures

4.1.1. Brittle-ductile deformation features

During the westward thrust motion of the PFT, the Tête d'Oréac cross-section passes through the PFT (Fig. 3) and preserves a succession of units that were stacked on each other. The main schistosity (S1) is parallel to the initial bedding (S0) in Cretaceous calcschists. S0-S1 is sub-horizontal and penetrative throughout the studied area. At the outcrop scale, S1 is clearly visible and shows dissolution surface with the development of stylolitic joints (Fig. 4).



209 **Fig. 4. a:** General sketch of sample FP18-1 evidencing cross-cutting relationships for two main vein generations
210 *fig. 3.c. b-d:* Microscope and cathodoluminescence pictures showing the different vein calcite generations.
211 Quartz anisotropy is observable in LPA which indicates an important deformation syn-post V1. This
212 suggests a strong transposition of structures during PFT compressional motion or the veins opened
213 initially in an orientation parallel to S1 either way a ductile deformation is recorded. These early

214 **shortening** features are cross-cut by numerous steeply dipping eastward normal faults linked to the
215 extensional reactivation of PFT. Early stages of extension are featured by centimetre scale “en-echelon”
216 veins (V2) indicative of an early brittle-ductile extensional deformation followed by dissolution on the
217 horizontal composite (S0-S1) cleavage. Larger V2 veins, expressed at centimetre scale, cross-cut the
218 cleavage and show elongated calcite fibres of ~1000 µm at the vein walls (Fig. 4). Similar shades for
219 early V2 and fibrous V2 are observed in CL. At vein cores, the fibrous calcite is then replaced by a
220 blocky calcite that is less luminescent in CL.

221

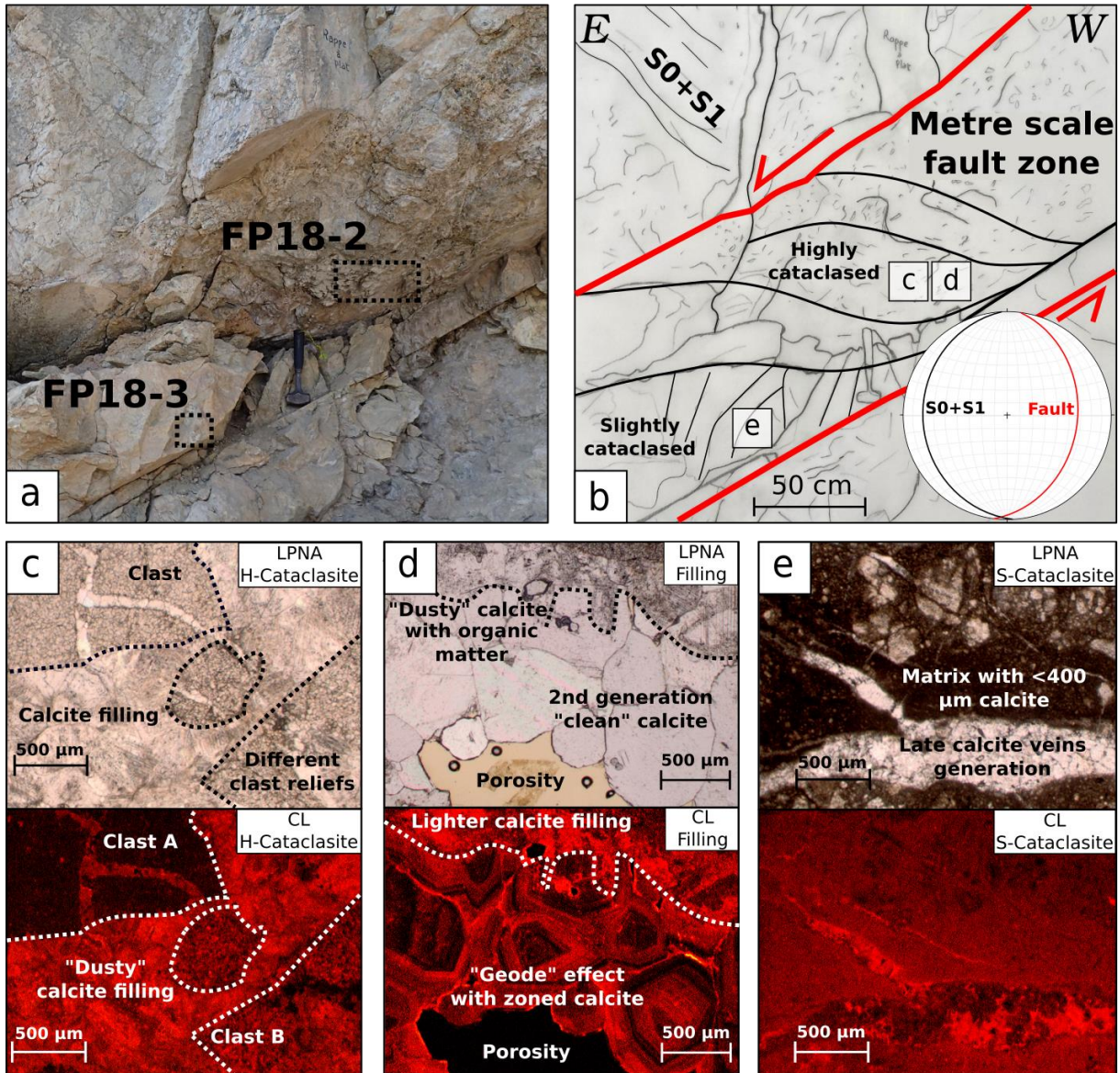
222 4.1.2. Brittle deformation features

223 The internal structure of one major extensional fault is investigated in the Tournoux scarp (Fig. 5). The
224 fault zone is highlighted by a metre-scale cataclasite fault gouge with variable amounts of deformations.
225 The top-to-the East (N90°E) normal sense of shear is represented by sigmoids and down-dip slickenside.
226 At thin-section scale, for sample FP18-2, the cataclasite is composed of centimetre-scale host rock clasts
227 with very small (<20 µm) limestone grains. Two types of calcite fillings have been identified. The first
228 one contains organic matter has a « dusty appearance » with bright shades in CL (Fig. 5C). The second
229 one shows large and clear crystals that grew in the cracks and porosity, showing sector zoning patterns
230 highlighted in CL and Laser Ablation-Inductively Coupled Plasma-Mass Spectrometry (LA-ICP-MS)
231 maps (Fig. 5D; Suppl. Mat. 3). ~700 µm large hexagonal, clear and organic matter free, calcite crystals
232 have been selected for U-Pb dating.

233 These calcite crystals represent the latest pervasive fluid circulation episode through the porosity and
234 provide a minimum age for the cataclasite. In sample FP18-3, the matrix is cross-cut by calcite veins
235 with variable diameters (300-1300 µm) and is free of any further deformation. On the basis of their
236 homogeneity and their youngest relative age relationships, these late calcites have also been targeted for
237 U-Pb calcite dating (see section 4.3). Samples FP19-12A-B (described in supplementary data) were
238 collected in a west-dipping conjugate normal fault and exhibits similar deformation features.

239

240 **Fig. 5. a-b:** Outcrop interpretation of the Tournoux scarp showing various degrees of cataclasis in Triassic
241 dolomitic limestone with Wulff stereogram lower hemisphere. Squares are sampled area, sample FP18-2 is a
242 highly cataclased sample, while sample FP18-3 is less intensely cataclased and is cross-cut by millimeter-scale
243 calcite veins. **c, d, e:** Microscope and cathodoluminescence pictures showing several calcite filling generations.
244 « clear calcite » shows zonings and seems to crystallize into a primary porosity left within the cataclasite. The
245 clear calcite and veins from the cataclasite are dated using the U-Pb dating on calcite method.



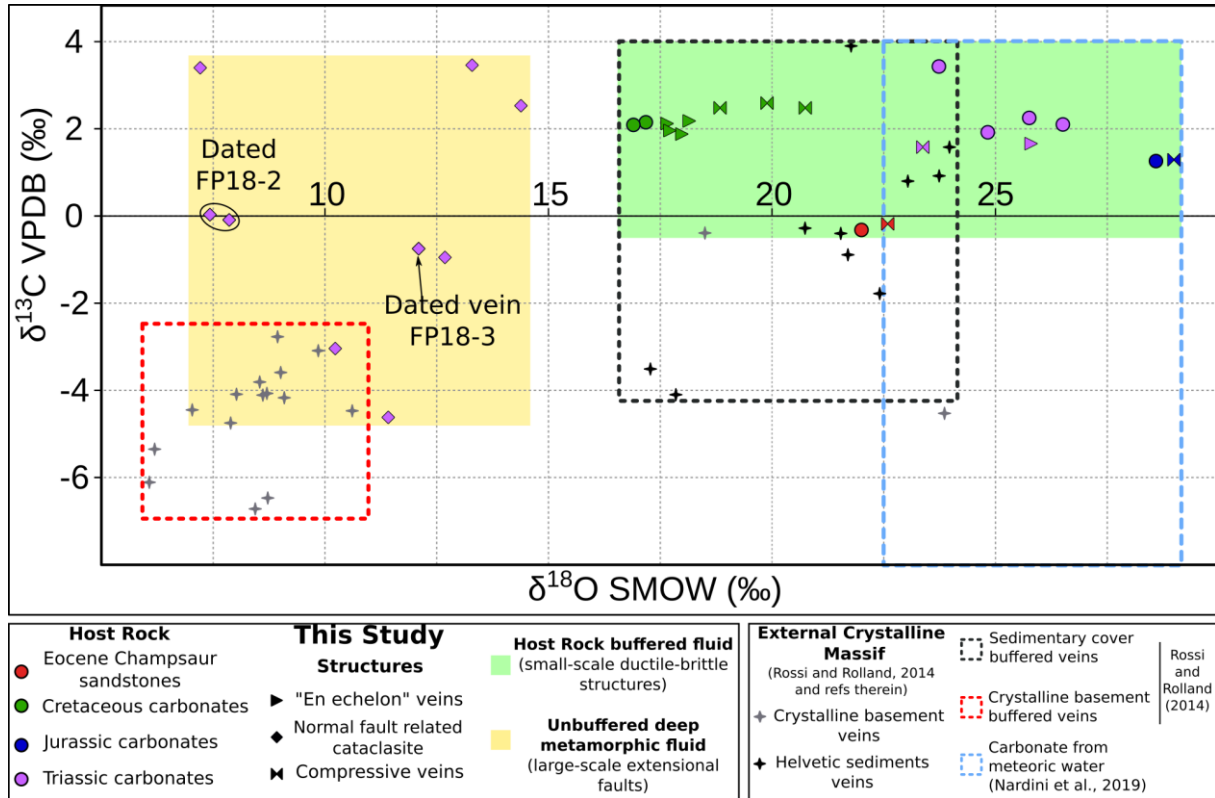
246

247 *4.2. $\delta^{13}\text{C}$ and $\delta^{18}\text{O}$ stable isotope results*

248 Stable isotopes analyses were performed in calcites from various host rocks samples belonging to the
 249 different units highlighted in the studied PFT section (Fig. 3) and are supposed to be representative of
 250 the different (compressional and extensional) key tectonic phases (Fig. 6).

251 For host rock analysis, upper Cretaceous planktonic calcschists from the Tête d'Oréac show the lowest
 252 $\delta^{18}\text{O}$ host rock value of 16.8-17.1 ‰ and of $\delta^{13}\text{C}$ of 2.1-2.2 ‰. Triassic carbonates show a range between
 253 23.7-26.5 ‰ for $\delta^{18}\text{O}$ and between 1.9-2.3 ‰ for $\delta^{13}\text{C}$ (with a higher value of 3.4 ‰ for the Ponteil
 254 scarp). Upper Jurassic calcschists gave $\delta^{18}\text{O}$ ratio of 28.5 ‰ and $\delta^{13}\text{C}$ of 1.3 ‰. The western Late Eocene
 255 Flysch (Champsaur sandstone) gave lowest $\delta^{13}\text{C}$ ratio of -0.3 ‰ and a $\delta^{18}\text{O}$ ratio of 21.9 ‰. Analysed
 256 brittle-ductile veins either related to the compressional or to the onset of the extensional tectonic phases
 257 stand very close to their host rocks, near to the meteoric water field defined by Nardini et al. (2019)

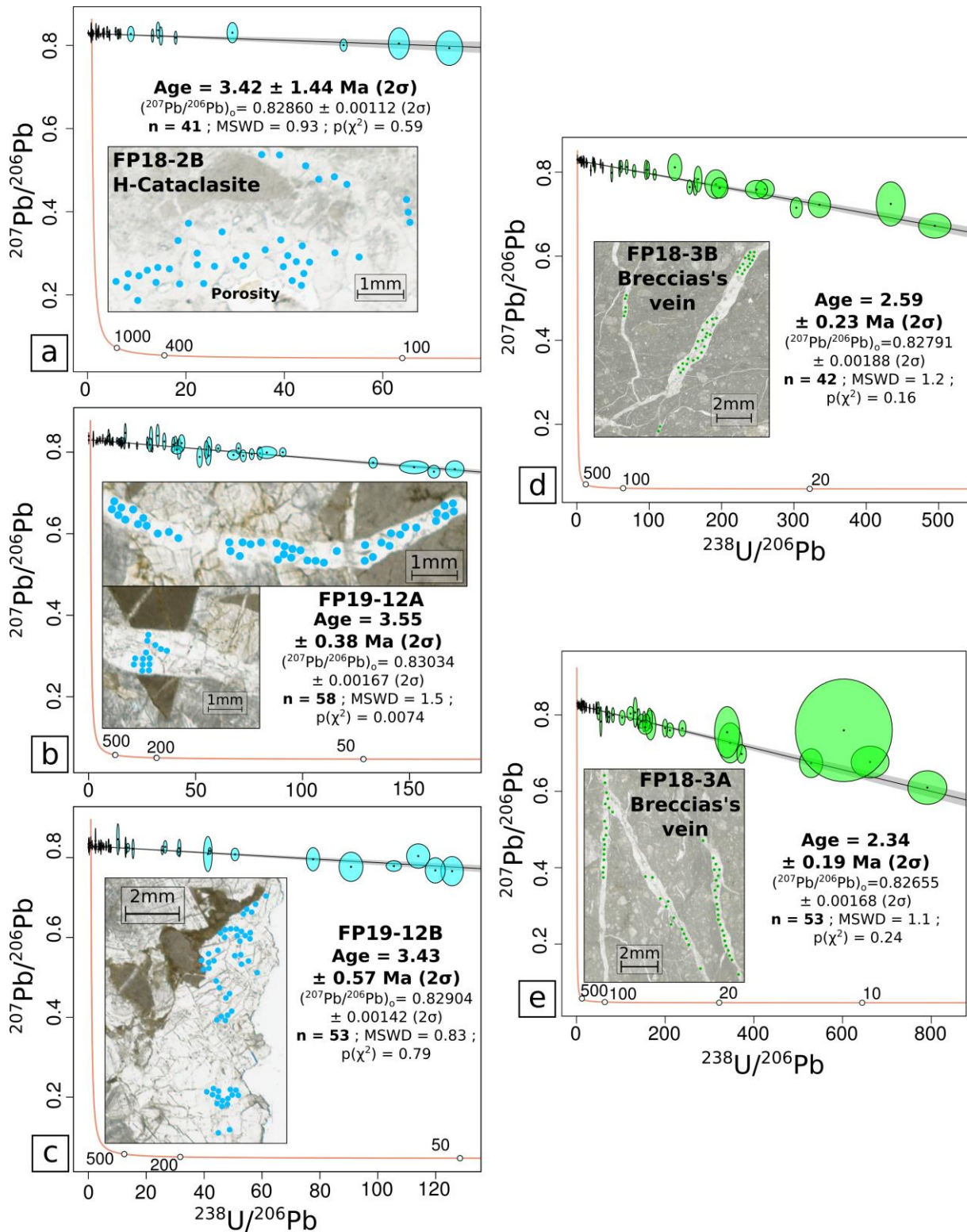
258 (Fig. 6). However, the V2 veins associated to the brittle normal fault development, clearly show lower
 259 $\delta^{18}\text{O}$ values ($<15\text{‰}$) compared to their host rocks, with a trend towards lower $\delta^{13}\text{C}$ values. These isotope
 260 signatures are similar to those measured in calcite from veins of the Mont Blanc External Crystalline
 261 Massifs (Rossi and Rolland, 2014).



262 **Fig. 6.** Stable isotopic data from samples indicated on Fig. 2. Domains represented by dashed red, black and blue
 263 lines are from the literature (Nardini et al., 2019; Rossi and Rolland, 2014 and references therein). The coloured
 264 green domain corresponds to veins associated to brittle-ductile structures. These veins show similar isotopic
 265 compositions as their host rocks. The orange domain features the signature of cataclased normal fault samples,
 266 which show a different isotopic composition as compared to their host rock, and are similar to deep metamorphic
 267 fluids (e.g., Crespo-Blanc et al., 1995; Rossi and Rolland, 2014; Rolland and Rossi, 2016).

268 4.3. Calcite LA-ICPMS U-Pb dating results

269 Petrographic analysis has been complemented by screening using LA-ICP-MS on 24 thin-sections from
 270 samples of 7 locations around the PFT related to **shortening** and **extensional** structures. Among these,
 271 20 screened samples show high common lead contents, and sometimes higher lead to uranium intensity
 272 signals. U-Pb dating of such carbonates with high lead concentrations remains highly challenging,
 273 especially for very young samples. However, four samples (samples FP18-2, 3 and FP19-12A&B
 274 described in section 4.1 and supplementary data) from the Tournoux normal fault site bear sufficient
 275 ^{238}U ($\sim 0\text{--}8.5$ ppm for FP18-3A&B and $\sim 0\text{--}4.5$ ppm for FP18-2B and FP19-12A&B), and ^{206}Pb , ^{207}Pb
 276 ($\sim 0\text{--}1.9$ ppm for FP18-3A&B and $\sim 0\text{--}13.1$ ppm for FP18-2B and FP19-12A&B).



278 **Fig. 7.** Tera-Wasserburg concordia plot of (a) Highly cataclased sample FP18-2 calcite filling (b) and (c) sample
 279 FP19-12A veins and FP19-12A 'clean calcite' filling (d) and (e) sample FP18-3 veins, and corresponding maps
 280 of sampled spots (150 μm). MSWD: Mean Square Weighted Deviation. An additional error propagation tied to
 281 WC-1 standard uncertainty is taken into account.
 282

283 Lead contents are based on NIST614 intensities and uranium contents are based on WC-1 intensities
284 (Jochum et al., 2011; Roberts et al., 2017; Woodhead et al., 2001), giving measurable and significant
285 radiogenic signal. Five ages have been obtained on these four samples (Fig. 7).

286 A first group of ages of ~ 3.5 Ma is represented by three samples. The cataclasite ‘clean calcite’ infill
287 (sample FP18-2B; Fig. 5) gives age of 3.42 ± 1.44 Ma ($n=41$, MSWD=0.93). This quite large uncertainty
288 is due to a relatively moderate U/Pb variability and the resulting low radiogenic signal measurable in
289 this sample. Samples FP19-12A&B give two similar within-error ages for the vein calcite and ‘clean
290 calcite’ infill, of 3.55 ± 0.38 ($n=58$, MSWD=1.5) and 3.43 ± 0.57 ($n=53$, MSWD=0.83), respectively.

291 A second group of ages of ~ 2.5 Ma is obtained on different cross-cutting veins of the latest generation
292 of sample FP-18-3 (Fig. 5), represented by slightly younger, but distinct out of error margins, ages of
293 2.59 ± 0.23 Ma ($n=42$, MSWD=1.2; FP-18-3B in Fig. 7b) and 2.34 ± 0.19 Ma ($n=53$, MSWD=1.1; FP-18-
294 3B in Fig. 7c). The higher spread in U/Pb ratios measured in these two latter ages results in more precise
295 and robust ages. These two age groups obtained on extensional faults connected to the PFT highlight
296 for the first time at least two phases of deformation constrained out of error bars: a first phase of brittle
297 deformation forming the cataclasite at 3.5 ± 0.4 and one or two discrete brittle events at, or comprised
298 within, 2.6 ± 0.2 and 2.3 ± 0.2 Ma. These ages show that the sated conjugated faults have been active for
299 at least 1 Myr, and are featured by only several datable events, representing co-seismic motions on the
300 faults.

301

302 5. Discussion

303 Onset of extensional tectonics in the Alps has remained a topic of debate for the last 20 years. A Miocene
304 age has been proposed for the onset of the extensional activation of the PFT based on AFT datings on
305 both sides of this major fault, i.e. in the Pelvoux External Crystalline Massif and in the Champsaur
306 sandstones to the west and in the Briançonnais zone to the east (Tricart et al., 2001; 2007; Beucher et
307 al., 2012). The Briançonnais zone corresponds to the east hanging wall compartment of the PFT. In this
308 compartment, AFT ages ranging from 30 Ma to 20 Ma are interpreted as the exhumation age of this area
309 related to the compressional activity of the PFT during the Alpine collision, which motion is constrained
310 by direct $^{40}\text{Ar}/^{39}\text{Ar}$ dating on phengite at 35-25 Ma (Simon-Labric et al., 2009; Bellanger et al., 2015).
311 To the west (footwall of the PFT), the AFT ages range from 13 Ma to 4 Ma in the Pelvoux External
312 Crystalline Massif (Beucher et al., 2012), and from 9 to 4 Ma in the Champsaur sandstones (Tricart et
313 al., 2007), and are interpreted as the extensional reactivation of the PFT by these latter authors. As the
314 AFT dates record an exhumation age associated with cooling below $\sim 100^\circ\text{C}$ (Ault et al., 2019), they
315 may not correspond to an age of PFT activity but rather record an erosion process that is related to both
316 climatic and tectonic processes (e.g., Champagnac et al., 2007). Sternai et al. (2019) suggest that vertical
317 movement in the Western Alps may be mainly ascribed to erosion and deglaciation (Nocquet et al.,

318 2016) and may also include a significant mantle convection component (Salimbeni et al., 2018).
319 However, the External Crystalline Massifs exhumation was also driven by frontal thrusting, activated
320 during middle Miocene at the western front of these massifs (Boutoux et al., 2015) and by strong
321 erosional processes that enhanced exhumation since the Late Miocene (Cederbom et al., 2004). Along
322 the PFT, younger AFT and phengite $^{40}\text{Ar}/^{39}\text{Ar}$ ages of ~10 Ma were obtained on the Plan de Phasy
323 (Guillestre) metagranite mylonites (Tricart et al., 2007; Lanari et al., 2014). These ages have been
324 interpreted as the result of hydrothermal fluid circulation, which may be linked to tectonic activity of
325 the High-Durance Fault System. However these fluid circulations may be passive through the PFT
326 network and may not correspond to extension onset. Therefore, the age of PFT activity remains
327 unconstrained and requires some direct datings. In the following discussion, we show how absolute U-
328 Pb dating of fracture infill calcite brings quantitative time constraints on PFT fault movement.

329

330 *5.1. Deformation and scale of fluid flow in the brittle-ductile structures*

331 The measured $\delta^{18}\text{O}$ and $\delta^{13}\text{C}$ isotope ratios of veins from brittle-ductile structures are close or similar to
332 their host rocks, and remain close to the field of carbonates precipitated from meteoric water (section
333 4.2). Based on several studies in the frontal parts of Alpine orogens (Smeraglia et al., 2020; Nardini et
334 al., 2019), these isotope signatures are thought to be representative of meteoric water inflow from the
335 most superficial domains. Three important parameters are involved to control this surface-derived fluid
336 regime: (i) lack of large-scale structures (ii) pressure-solution microstructures (evidence of local fluid)
337 (iii) presence of a shallow impermeable clay-rich layers which isolate upper crust from more deeply-
338 rooted systems (section 4.1. and Fig. 3). Rossi and Rolland (2014) report similar stable isotope
339 signatures in the Mont Blanc External Crystalline Massif sedimentary cover (Helvetic schists). There,
340 the vein calcites bear similar stable isotope values as the host Helvetic schists, which is in agreement
341 with the fluids to have equilibrated with their host rocks in a closed system with low fluid/rock ratios
342 (Rolland and Rossi, 2016). In our study, observations of veins show that they were closely related to
343 schistosity acting as a stylolitic dissolution surface (section 4.1). This observation is consistent with
344 local fluid interactions and equilibrium with the host rock, resulting from a pressure-dissolution-
345 recrystallization transfer mode (e.g. Passchier and Throw, 2005). Based on this, we suggest that the
346 external fluid signature was buffered by the host rock signature. These fluid compositions show that ‘en-
347 echelon’ veins are linked to an early deformation, where the porosity was still not connected by the fault
348 network (Fig. 3). In such a system, the veins kept the host rock signature and no crustal-scale fluid flow
349 circulation is evidenced.

350

351 *5.2. Scale of fluid flow in the brittle extensional structures*

352 Major (> metre-scale width) faults are related to shallower, or higher stress contexts (e.g. Passchier and
353 Throw, 2005). The isotopic composition of calcite that crystallised in these brittle extensional faults is
354 significantly different from their host rock (section 4.2; Fig. 6). Indeed, calcites related to these major
355 faults have $\delta^{18}\text{O}$ lower than 10 ‰ from their host rock and a $\delta^{13}\text{C}$ ranging between -5 to 4 ‰ PDB (while
356 the $\delta^{13}\text{C}$ ratio of Trias host rock is of 2 ‰). This signature is similar to that of exogenous metamorphic
357 fluid origin (Crespo-Blanc et al., 1995; Rossi and Rolland, 2014). The observed CL pattern of calcites
358 also argues for variations in the fluid composition, between the different veins and progressively within
359 a given vein. Similar signatures are recorded in the Mont Blanc External Crystalline Massif shear zones
360 and veins in a similar structural context (Rossi et al., 2014). There, a similar spread of $\delta^{13}\text{C}$ - $\delta^{18}\text{O}$ values
361 is observed in the marginal part of the crystalline basement, at the contact with the Helvetic schists. This
362 spread is interpreted as a mixing between fluids flowing down through the sedimentary cover and
363 upwards fluids originating from shear zones in **the Mont Blanc Massif's central** (Rolland and Rossi,
364 2016). The chemical signature of calcite veins in the Massif Central shear zones is correlated to a Mg-
365 K-rich metasomatism, both arguing for CO_2 -bearing fluids representative of a deep source, which is
366 rooted in the mantle via vertical shear zones (Rossi et al., 2005). This deeply rooted fluid cell is also
367 suggested by fluids significantly hotter (150-250 °C) than their host-rock at ca. 10 Ma along vertical
368 faults in Belledonne Massif, which are in continuity with the central Mont Blanc Massif shear zones
369 (Janots et al., 2019). Indeed, deep metamorphic fluid circulation is in good agreement with a crustal-
370 scale fluid pathway which is activated during the extensional motion of the PFT, connected to the
371 Rhône-Simplon right-lateral fault (Bergemann et al., 2019; 2020). This crustal-scale network suggests
372 that extensional faults are in-depth connected to the PFT, when it was reactivated as a detachment. Deep
373 connection with the PFT crustal scale structure (e.g. Sue et al., 2003) would allow fluid circulation from
374 interface of European slab with the deep subduction/collisional metamorphosed prism. In our study, the
375 isotopic dataset shows a significant difference between the deep fluids signature recorded by the Mont
376 Blanc veins (Rossi and Rolland, 2014; Rolland and Rossi, 2016) and the compositions of the veins
377 related to brittle-ductile structures (Fig. 6). This variability suggests a mixing process between the local
378 fluids trapped in the early extensional (closed system) and these exogenous fluids from a deep crustal
379 origin.

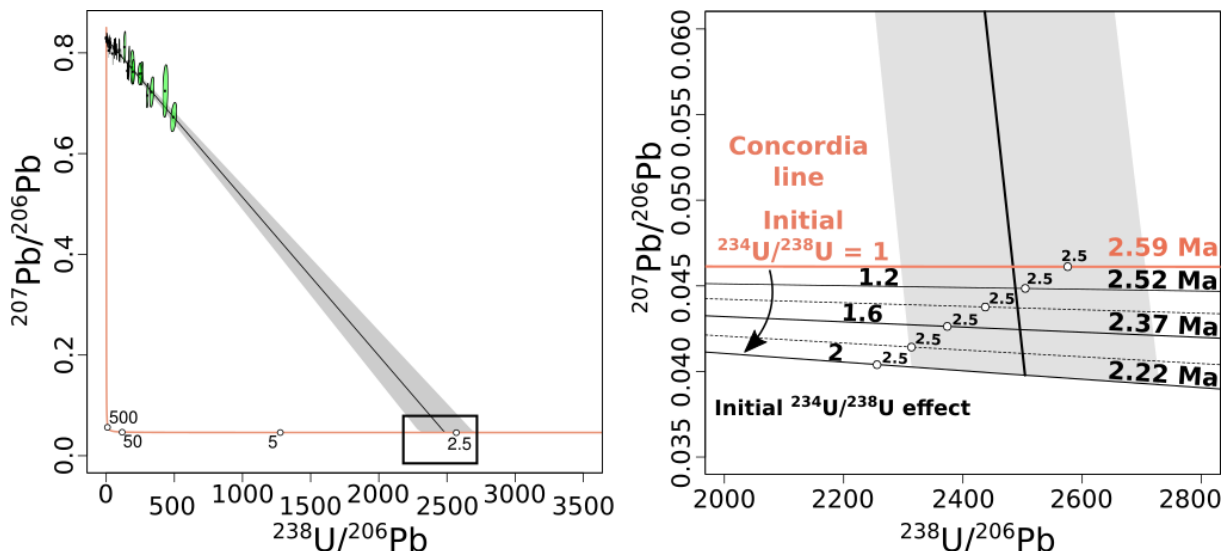
380

381

382 *5.3. Timing of PFT extensional inversion*

383 All ages obtained from the investigated Tournoux normal fault scarps, give direct time constraints on
384 the final stages of extensional slip, and are interpreted as a minimum age for the extensional reactivation
385 of the PFT. The oldest event is the formation of the highly deformed cataclasite calcite filling/veins ~3.5
386 Ma (3.4 ± 1.5 Ma, 3.6 ± 0.4 and 3.4 ± 0.6). This calcitic cementation occurred directly after the main

387 cataclastic deformation event and before the late cross-cutting veins. Latter cross-cutting veins gave the
 388 same ~ 2.5 Ma age, with two within-error dates of 2.6 ± 0.3 and 2.3 ± 0.3 Ma. The ~ 3.5 Ma and ~ 2.5 Ma
 389 do not represent the same slip event on the fault. It is noteworthy that all these ages are calculated
 390 assuming secular equilibrium in the U-series decay chain. As fluids are generally characterized by an
 391 excess in ^{234}U with respect to ^{238}U , resulting in an excess of radiogenic ^{206}Pb , the calculated ages should
 392 be considered as maximum ages (see for example Walker et al., 2006). The magnitude of the offset ages
 393 due to initial $^{234}\text{U}/^{238}\text{U}$ disequilibrium can be significant and the true age could be younger by several
 394 hundreds of thousands of years. In the present case, it was not possible to carry out classical isotopic
 395 analyses of uranium by isotopic dilution to measure any detectable residual $^{234}\text{U}/^{238}\text{U}$ disequilibrium
 396 because of the size of the carbonate phases. It could be hazardous to speculate on the initial $^{234}\text{U}/^{238}\text{U}$
 397 disequilibria of the fluids, but the quite high uranium concentrations (up to the ppm level) observed in
 398 analysed minerals of samples FP-18-2 & 3 (Fig. 7) are likely indicative of an oxidizing environment and
 399 thus of a moderate initial ^{234}U excess (Walker et al., 2006). To assess the impact of this excess on the
 400 final age, we have tested various initial $^{234}\text{U}/^{238}\text{U}$ activity ratios ranging between 1 to 2 as illustrated in
 401 Figure 8. For an initial ($^{234}\text{U}/^{238}\text{U}$) activity ratio of 2, the true age is lower by about ~ 370 ka. The obtained
 402 ages assuming an initial ($^{234}\text{U}/^{238}\text{U}$) ratio of 1 are thus regarded as maximum ages.
 403 As they remain undeformed, the latter veins are considered as the youngest tectonic slip along the fault.
 404 Furthermore, the geometry of the Tournoux normal fault regarding the PFT position indicates that this
 405 normal fault was connected to the PFT, which acted as a detachment Zone (Fig. 9). Thus, it may
 406 represent the paleo-HDFS seismogenic zone, which was later exhumed in the footwall part of the active
 407 extensional fault. Main activity of this paleo-fault can be bracketed between 3.4-2.2 Ma based on the
 408 above results.



409 **Fig. 8.** Impact of the initial ^{234}U excess on the final age estimation. Several initial $^{234}\text{U}/^{238}\text{U}$ activity
 410 ratios have been tested ranging between 1 to 2. This spread in initial $^{234}\text{U}/^{238}\text{U}$ leads to an age difference

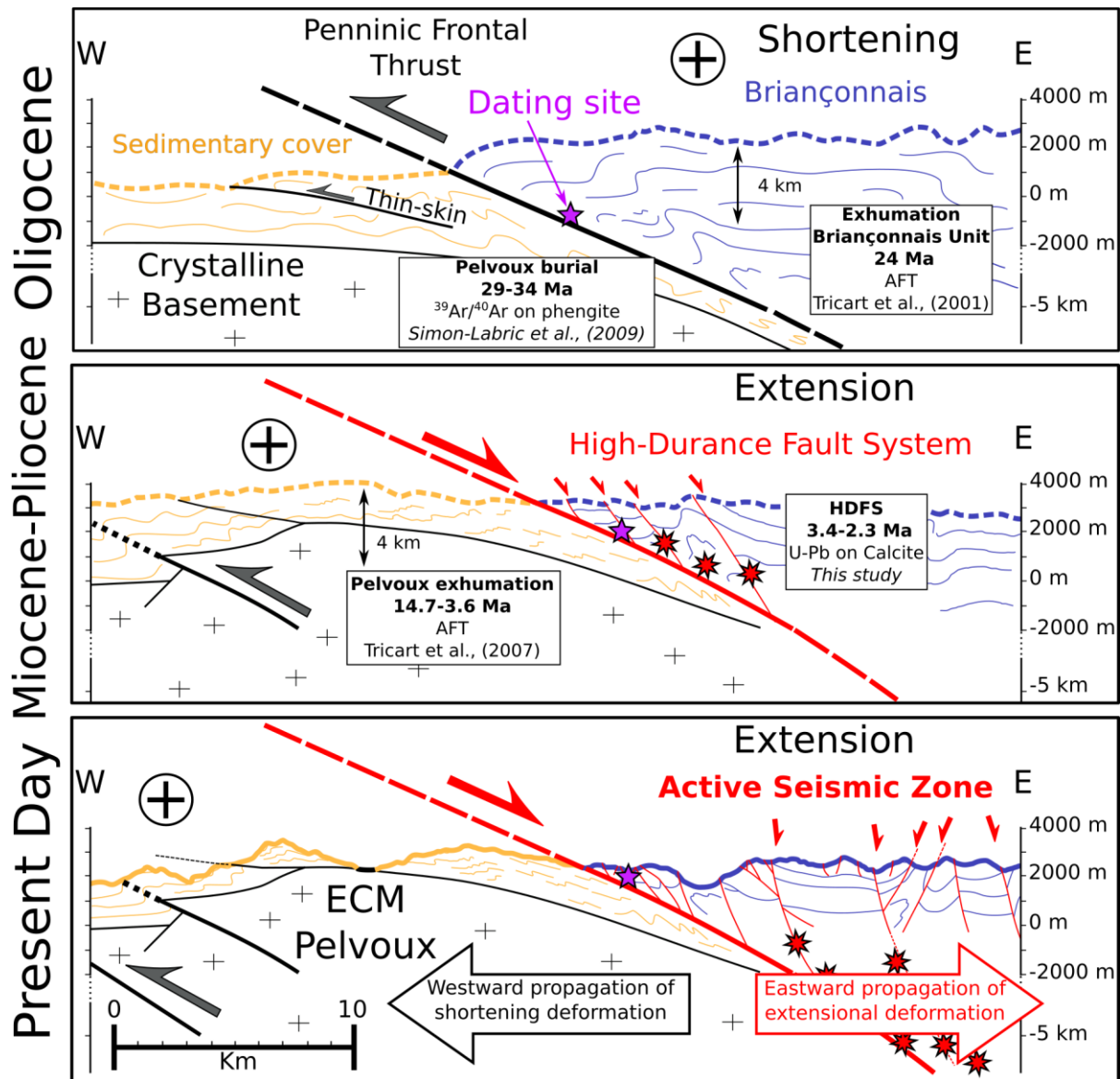
411 of 0.37 Ma. The obtained U/Pb age of 2.59 Ma, assuming equality of ^{234}U and ^{238}U contents is thus a
412 maximum age.

413

414 5.4. Evolution of PFT through time

415 The structural and dating results presented in this paper, combined with the literature on PFT footwall
416 and hanging wall exhumation lead to the following reconstitution of its evolution (Fig. 9).

417 The investigated PFT paleoseismic zone is located 3 to 10 km west of the active HDFFS seismogenic
418 zone. Nowadays, the extensional deformation is mainly localised on one active fault and mostly occurs
419 mostly at 3 to 8 km depth (Sue et al., 2007; Mathey et al., 2020). This study gives insights into the uplift
420 rate and lateral displacement of the High-Durance Fault System footwall and hanging wall since the
421 passage of the investigated paleo-PFT through the upper boundary of the seismogenic crust some 2-3.5
422 Ma ago. Since then, the PFT hanging wall, represented by the active extensional deformation front of
423 the HDFFS was significantly shifted eastward, while its footwall was uplifted up to 3 km (Fig. 9). This
424 leads to a mean vertical tectonic motion on the order of $> 1 \text{ mm.yr}^{-1}$ for the footwall compartment of
425 PFT on this period of time. This rate is consistent with the vertical GPS rates measured for the Pelvoux
426 External Crystalline Massif (Nocquet et al., 2016; Sternai et al., 2019).



427 **Fig. 9.** Evolutionary geological cross-section sketch of PFT (modified from Tricart et al., 2006). **a**, Compressional
 428 activation of the PFT resulting in joint External Crystalline Massifs burial and Briançonnais exhumation during
 429 the Oligocene. **b**, Extensional reactivation of the PFT and setting up of the High-Durance Fault System during the
 430 Pliocene as evidenced in this study. At this point the dated extensional fault passes through the upper boundary of
 431 the seismic zone at ca. 2-3 Ma. **c**, At present-day, compressional deformation has migrated westward (frontal part
 432 of External Crystalline Massifs, since c. 15 Ma) and extensional seismic activity of the High-Durance Fault System
 433 is recorded at shallow depth 3-10 km east of the studied paleoseismic zone.

434
 435 Our data support the hypothesis that the present HDFS is the result of eastward shifting of extensional
 436 deformation, accommodated by successive jumps on several faults. Faults were likely active on a scale
 437 of ≥ 1 Myr before becoming inactive. Calcite U-Pb ages obtained on the Tournoux scarp constrain co-
 438 seismic motion on two conjugate faults. The two age groups obtained on these extensional faults
 439 connected to the PFT highlight at least two phases of deformation, at 3.5 ± 0.4 Ma and one or two discrete

440 brittle events at, or comprised within, 2.6 ± 0.2 and 2.3 ± 0.2 Ma, which gives insights into the long-term
441 activity of the of at least 1 Myr, but with only several datable events, which argues for an apparent
442 contradiction. Indeed, co-seismic displacement on the fault suggest a significant magnitude for the
443 related earthquake (Wells and Coppersmith, 1994), which is apparently incompatible with the very few
444 datable motions. This gives some weight to a deformation regime which may alternate long phases of
445 creeping on the fault plane, without any brittle deformation, with very rare phases of brittle deformation.
446 The vertical uplift and exhumation of the Pelvoux External Massif since 3.5 Ma may thus mainly result
447 from the cumulated fault motion on these several fault segments. These data are thus in agreement with
448 a significant tectonic component in the measured uplift signal of External Crystalline Massifs, which is
449 in agreement with a clear difference in uplift rates measured between ECMs and Internal Alps (Nocquet
450 et al., 2016; Sternai et al., 2019).

451 We support the hypothesis that the HDFs is the result of the eastward extensional deformation shift and
452 the successive activation of faults, which incrementally participated at the exhumation of the western
453 (Pelvoux) footwall side of the fault system.

454

455 **6. Conclusion**

456 Significant constraints on the evolution of fault systems can be acquired by coupling stable isotopic
457 analysis and U-Pb dating on calcite. These methods have been successfully applied to unravel the
458 tectonic reactivation of the PFT for the first time. Five U-Pb ages on calcite have been obtained on
459 extensional fault structures connected to the PFT, gave two distinct groups of ages of 3.5 ± 0.5 Ma for
460 the main deformation phase represented by the cataclasite calcite cement, cross-cut by later discrete
461 phases represented by mm-large veins dated from 2.6 ± 0.3 to 2.3 ± 0.3 Ma. The 3.5 Ma age represents a
462 minimum age for the onset of extensional brittle reactivation of the PFT. Earliest extensional ductile-
463 brittle structures cannot be dated due to low uranium contents and low U/Pb ratios. Associated to those
464 two (ductile and brittle) deformation stages, stable isotopic ratios of carbon ($\delta^{13}\text{C}$) and oxygen ($\delta^{18}\text{O}$) of
465 calcite samples collected within the kilometre-scale extensional faults show an evolution from a closed
466 to an open fluid system. The isotopic signature of fluids related to the brittle deformation stage
467 corresponds an open system due to the activation of a crustal-scale fluid circulation cell when the HDFs
468 developed in connection with the deeper PFT deeper structure. The fluids associated to this open system
469 show a deep crustal/mantle signature similar to that measured along the PFT across the Alpine arc. This
470 deeply rooted upward fluid circulation occurred when extensional fault activity was connected to the
471 PFT reactivated as a detachment, which suggests a crustal-scale extensional reactivation at this stage.
472 These constraints on PFT fluid regime are the first direct evidence for a transition towards a crustal-
473 scale fluid regime at the onset of brittle extensional reactivation in the Alps. The direct ages of PFT
474 motion give insights into the long-term incremental displacement of the HDFs footwall, and Pelvoux

475 Massif exhumation, which corresponds to its passage through the upper part of the seismogenic zone, at
476 a mean rate of $> 1 \text{ mm.yr}^{-1}$ in the last 3 Ma.

477

478 **Acknowledgements**

479 This work forms part of first author's Ph.D. funded by the BRGM in the frame of the RGF project. The
480 CEREGE group is supported by 2 French "Investissements d'Avenir" fundings: the EQUIPEX-ASTER-
481 CEREGE and the Initiative d'Excellence of Aix-Marseille University - A*Midex, through the DatCarb
482 project. We wish to thank Fayçal Soufi for his help in sample preparation.

483 **Many thanks are due to Alfons Berger, anonymous reviewer and Giancarlo Molli for their constructive**
484 **comments which improved the manuscript.**

485

486 **Author contributions**

487 AB, YR and SS wrote the manuscript and all authors discussed the results and contributed to the final
488 article. TD supported AB for map creation and cross-sections. YR, SS, TD, CG and AB participated to
489 field trip sampling. AB did the sample petrographic characterization with optical microscope and
490 cathodoluminescence. NG, AG and PD led U-Pb dating with AB. BB and AN supervised AB for stable
491 isotopes analysis, for results interpretation and protocol application respectively.

492

493 **Supplementary Materials**

494 Suppl. Mat. Table S1. Sample locations and descriptions.

495 Suppl. Mat. Fig. S1. Tournoux's scarp general view.

496 Suppl. Mat. Fig. S2. Field photographs FP19-12 site.

497 Suppl. Mat. Fig. S3. La-ICPMS elemental maps, FP18-2B.

498 Suppl. Mat. Fig. S4. FP19-12B thin section with map localisation.

499 Suppl. Mat. Fig. S5. La-ICPMS elemental map, FP19-12B.

500

501 Suppl. Mat. Table S2. U-Pb on calcite La-ICPMS data.

Table 1: Isotopic composition of analysed calcites

	N°Sample	$^{13}\delta\text{C PDB}$	$^{18}\delta\text{O SMOW}$	
<i>Whole Rock</i>	FP18-1A	2,15	17,18	
	FP18-1A	2,09	16,90	
	FP18-4	1,92	24,83	
	FP18-7	2,25	25,76	
	FP18-9	-0,32	22,00	
	FP18-10	1,26	28,59	
	FP18-11	2,1	26,51	
	FP18-13	3,43	23,73	
	<i>Early veins (V1)</i>	FP18-1B	2,59	19,89
		FP18-1C	2,48	20,74
		FP18-1C	2,48	18,84
		FP18-9	-0,18	22,59
		FP18-10	1,29	28,99
FP18-11		1,58	23,37	
<i>En-echelon veins (V2)</i>	FP18-1A	2,12	17,65	
	FP18-1A	2,18	18,15	
	FP18-1B	1,96	17,71	
	FP18-1D	1,88	17,98	
	FP18-5	1,66	25,80	
<i>Cataclasite infill (V2)</i>	FP18-2A	0,03	7,43	
	FP18-2B	-0,09	7,86	
	FP18-3B	-4,62	11,41	
	FP18-3B	-0,75	12,10	
	FP18-6	-3,04	10,23	
	FP18-6	-0,95	12,68	
	FP18-13	3,46	13,29	
	FP18-13	2,53	14,38	
	FP18-13	3,4	7,21	

502

Table 1. *Stable isotope data from host rocks, calcite veins and cataclasite fillings of extensional faults.*

503 **Références**

- 504 Andrieu, S., Brigaud, B., Rabourg, T., and Noret, A.: The Mid-Cenomanian Event in shallow marine
505 environments: Influence on carbonate producers and depositional sequences (northern Aquitaine
506 Basin, France), *Cretaceous Res.*, 56, 587–607, <https://doi.org/10.1016/j.cretres.2015.06.018>, 2015.
- 507 Ault, A. K., Gautheron, C., and King, G. E.: Innovations in (U–Th)/He, fission track, and trapped
508 charge thermochronometry with applications to earthquakes, weathering, surface- mantle
509 connections, and the growth and decay of mountains, *Tectonics*, 38(11), 3705–3739,
510 <https://doi.org/10.2029/2018TC005312>, 2019.
- 511 Barnaby, R. J. and Rimstidt, J. D.: Redox conditions of calcite cementation interpreted from Mn and
512 Fe contents of authigenic calcites, *Geol. Soc. Am. Bull.*, 101(6), 795–804,
513 [https://doi.org/10.1130/0016-7606\(1989\)101<0795:RCOCCI>2.3.CO;2](https://doi.org/10.1130/0016-7606(1989)101<0795:RCOCCI>2.3.CO;2), 1989.
- 514 Beaudoin, N., Huyghe, D., Bellahsen, N., Lacombe, O., Emmanuel, L., Mouthereau, F., and
515 Ouahnon, L.: Fluid systems and fracture development during syn-depositional fold growth: An
516 example from the Pico del Aguila anticline, Sierras Exteriores, southern Pyrenees, Spain. *J. Struct.*
517 *Geol.*, 70, 23–38, <https://doi.org/10.1016/j.jsg.2014.11.003>, 2015.
- 518 Beaudoin, N., Lacombe, O., Roberts, N.M.W., and Koehn, D.: U-Pb dating of calcite veins reveals
519 complex stress evolution and thrust sequence in the Bighorn Basin, Wyoming, USA. *Geology*, 46,
520 1015–1018, <https://doi.org/10.1130/G45379.1>, 2018.
- 521 Bellahsen, N., Mouthereau, F., Boutoux, A., Bellanger, M., Lacombe, O., Jolivet, L., and Rolland, Y.:
522 Collision kinematics in the western external Alps, *Tectonics*, 33(6), 1055–1088,
523 <https://doi.org/10.1002/2013TC003453>, 2014.
- 524 Bellanger, M., Augier, R., Bellahsen, N., Jolivet, L., Monié, P., Baudin, T., and Beyssac, O.:
525 Shortening of the European Dauphinois margin (Oisans Massif, Western Alps): New insights from
526 RSCM maximum temperature estimates and $^{40}\text{Ar}/^{39}\text{Ar}$ in situ dating, *J. Geodyn.*, 83, 37–64,
527 <https://doi.org/10.1016/j.jog.2014.09.004>, 2015.
- 528 Beltrando, M., Lister, G.S., Forster, M., Dunlap, W.J., Fraser, G., and Hermann, J.: Dating
529 microstructures by the $^{40}\text{Ar}/^{39}\text{Ar}$ step-heating technique: Deformation–pressure–temperature–time
530 history of the Penninic Units of the Western Alps, *Lithos*, 113, 801–819,
531 <https://doi.org/10.1016/j.lithos.2009.07.006>, 2009.
- 532 Bergemann, C.A., Gnos, E., and Whitehouse, M.J.: Insights into the tectonic history of the Western
533 Alps through dating of fissure monazite in the Mont Blanc and Aiguilles Rouges Massifs,
534 *Tectonophysics*, 750, 203–212, <https://doi.org/10.1016/j.tecto.2018.11.013>, 2019.
- 535 Bergemann, C.A., Gnos, E., Berger, A., Janots, E., and Whitehouse, M.J.: Dating tectonic activity in
536 the Lepontine Dome and Rhone-Simplon Fault regions through hydrothermal monazite-(Ce), *Solid*
537 *Earth*, 11, 199–222, <https://doi.org/10.5194/se-11-199-2020>, 2020.
- 538 Bertrand, A. and Sue, C.: Reconciling late faulting over the whole Alpine belt: from structural analysis
539 to geochronological constrains, *Swiss J. Geosci.*, 110, 565–580, <https://doi.org/10.1007/s00015-017-0265-4>, 2017.
- 540

541 Beucher, R., van der Beek, P., Braun, J., and Batt, G.E.: Exhumation and relief development in the
542 Pelvoux and Dora-Maira analysis and inversion of thermochronological age transects, *J. Geophys.*
543 *Res.*, 117, F03030, <https://doi.org/10.1029/2011JF002240>, 2012.

544 Bons, P.D., Elburg, M.A., and Gomez-Rivas, E.: A review of the formation of tectonic veins and their
545 microstructures, *J. Struct. Geol.*, 43, 33–62. <https://doi.org/10.1016/j.jsg.2012.07.005>, 2012.

546 Boutoux, A., Bellahsen, N., Nanni, U., Pik, R., Verlaquet, A., Rolland, Y., and Lacombe, O.: Thermal
547 and structural evolution of the external Western Alps: Insights from (U–Th–Sm)/He
548 thermochronology and RSCM thermometry in the Aiguilles Rouges/Mont Blanc massifs,
549 *Tectonophysics*, 683, 109–123, <https://doi.org/10.1016/j.tecto.2016.06.010>, 2016.

550 Cederbom, C.E., Sinclair, H.D., Schlunegger, F., and Rahn, M.K.: Climate induced rebound and
551 exhumation of European Alps, *Geology*, 32, 709–712, <https://doi/10.1130/G20491.1>, 2004.

552 Cenki-Tok, B., Darling, J.R., Rolland, Y., Dhuime, B., and Storey, C.D.: Direct dating of mid-crustal
553 shear zones with synkinematic allanite: new in situ U-Th-Pb geochronological approaches applied
554 to the Mont Blanc massif, *Terra Nova*, 26, 29–37, <https://doi.org/10.1111/ter.12066>, 2014.

555 Ceriani, S., Fügenschuh, B., and Schmid, S. M.: Multi-stage thrusting at the " Penninic Front" in the
556 Western Alps between Mont Blanc and Pelvoux massifs, *Int. J. Earth Sci.*, 90(3), 685-702,
557 <https://doi.org/10.1007/s005310000188>, 2001.

558 Ceriani, S. and Schmid, S.M.: From N-S collision to WNW-directed post-collisional thrusting and
559 folding: Structural study of the Frontal Penninic Units in Savoie (Western Alps, France), *Eclogae*
560 *geol. Helv.*, 97, 347–369, <https://doi.org/10.1007/s00015-004-1129-2>, 2004.

561 Champagnac, J. D., Molnar, P., Anderson, R. S., Sue, C., and Delacou, B.: Quaternary erosion-
562 induced isostatic rebound in the western Alps, *Geology*, 35(3), 195-198,
563 <https://doi/10.1130/G23053A.1>, 2007.

564 Crespo-Blanc, A., Masson, H., Sharp, Z., and Cosca, M.: A stable and $^{40}\text{Ar}/^{39}\text{Ar}$ isotope study of a
565 major thrust in the Helvetic nappes (Swiss Alps): Evidence for fluid flow and constraints on nappe
566 kinematics, *Geol. Soc. Am. Bull.*, 107(10), 1129-1144, [https://doi.org/10.1130/0016-7606\(1995\)107<1129:ASAAAI>2.3.CO;2](https://doi.org/10.1130/0016-7606(1995)107<1129:ASAAAI>2.3.CO;2), 1995.

568 Duchêne, S., Blichert-Toft, J., Luais, B., Télouk, P., Lardeaux, J.-M., and Albarède, F.: The Lu–Hf
569 dating of garnets and the ages of the Alpine high-pressure metamorphism, *Nature*, 387, 586–589,
570 <https://doi.org/10.1038/42446>, 1997.

571 Dumont, T., Schwartz, S., Guillot, S., Simon-Labric, T., Tricart, P., and Jourdan, S.: Structural and
572 sedimentary records of the Oligocene revolution in the Western Alpine arc, *J. Geodyn.*, 56–57, 18–
573 38, <https://doi.org/10.1016/j.jog.2011.11.006>, 2012.

574 Goodfellow, B.W., Viola, G., Bingen, B., Nuriel, P., and Kylander-Clark, A.R.C.: Palaeocene faulting
575 in SE Sweden from U-Pb dating of slickenfibres calcite, *Terra Nova*, 29, 321–328,
576 <https://doi.org/10.1111/ter.12280>, 2017.

577 Janots, E., Grand'Homme, A., Bernet, M., Guillaume, D., Gnos, E., Boiron, M. C., Rossi, M.,
578 Seydoux-Guillaume, A.-M., and De Ascensão Guedes, R.: Geochronological and thermometric

579 evidence of unusually hot fluids in an Alpine fissure of Lauzière granite (Belledonne, Western
580 Alps), *Solid Earth*, 10(1), 211-223, <https://doi.org/10.5194/se-10-211-2019>, 2019.

581 Jochum, K. P., Weis, U., Stoll, B., Kuzmin, D., Yang, Q., Raczek, I., Jacob, D.E., Stracke, A.,
582 Birbaum, K., Frick, D.A., Günther, D., and Enzweiler, J.: Determination of reference values for
583 NIST SRM 610–617 glasses following ISO guidelines, *Geostand. Geoanal. Res.*, 35(4), 397-429.
584 <https://doi/10.1111/j.1751-908X.2011.00120.x>, 2011.

585 Kim, S.-T., Coplen, T.B., and Horita, J.: Normalization of stable isotope data for carbonate minerals:
586 Implementation of IUPAC guidelines, *Geochim. Cosmochim. Ac.*, 158, 276–289,
587 <https://doi.org/10.1016/j.gca.2015.02.011>, 2015.

588 Lanari, P., Guillot, S., Schwartz, S., Vidal, O., Tricart, P., Riel, N., and Beysac, O.: Diachronous
589 evolution of the alpine continental wedge: evidences from P-T estimates in the Briançonnais Zone
590 houillère (France-Western Alps), *J. Geodyn.*, 56-57, 39–54,
591 <https://doi.org/10.1016/j.jog.2011.09.006>, 2012.

592 Lanari, P., Rolland, Y., Schwartz, S., Vidal, O., Guillot, S., Tricart, P., and Dumont, T.: P-T-t
593 estimation of syn-kinematic strain in low-grade rocks (<300°C) using thermodynamic modelling
594 and ⁴⁰Ar/³⁹Ar dating techniques: example of the Plan-de-Phasy shear zone (Briançonnais Zone,
595 Western Alps), *Terra Nova*, 26, 130–138, <https://doi.org/10.1111/ter.12079>, 2014.

596 Lardeaux J.M., Schwartz S., Tricart P., Paul A., Guillot S., Béthoux N., and Masson F.: A crustal-scale
597 cross-section of the southwestern Alps combining geophysical and geological imagery, *Terra
598 Nova*, 18 (6), 412-422, <https://doi.org/10.1111/j.1365-3121.2006.00706.x>, 2006.

599 Larroque, C., Delouis, B., Godel, B., and Nocquet, J.-M.: Active deformation at the southwestern
600 Alps–Ligurian basin junction (France–Italy boundary): Evidence for recent change from
601 compression to extension in the Argentera massif, *Tectonophysics*, 467, 22–34,
602 <https://doi.org/10.1016/j.tecto.2008.12.013>, 2009.

603 Malusà, M., Zhao, L., Eva, E., Solarino, S., Paul, A., Guillot, S., Schwartz, S., Dumont, T., Aubert, C.,
604 Salimbeni, S., Pondrelli, S., Wang, and Q., Zhu, R.: Earthquakes in the western alpine mantle
605 wedge, *Gondwana Research*, 44, 89-95, <http://dx.doi.org/10.1016/j.gr.2016.11.012>, 2017.

606 Mathey, M., Walpersdorf, A., Sue, C., Baize, S., and Deprez, A.: Seismogenic potential of the High
607 Durance Fault constrained by 20 yr of GNSS measurements in the Western European Alps,
608 *Geophy. J. Int.*, 222(3), 2136-2146, <https://doi.org/10.1093/gji/ggaa292>, 2020.

609 Mugnier, J. L., Loubat, H., and Cannic, S.: Correlation of seismic images and geology at the boundary
610 between internal and external domains of the Western Alps, *Bull. Soc. Géol. Fr.*, 164(5), 697-708,
611 1993.

612 Nardini, N., Muñoz-López, D., Cruset, D., Cantarero, I., Martín-Martín, J., Benedicto, A., Gomez-
613 Rivas, E., John, C., and Travé, A.: From Early Contraction to Post-Folding Fluid Evolution in the
614 Frontal Part of the Bóixols Thrust Sheet (Southern Pyrenees) as Revealed by the Texture and
615 Geochemistry of Calcite Cements, *Minerals*, 9, 117, <https://doi.org/10.3390/min9020117>, 2019.

616 Nocquet, J. M., Sue, C., Walpersdorf, A., Tran, T., Lenôtre, N., Vernant, P., Cushing, M., Jouanne, F.,
617 Masson, F., Baize, S., Chéry, J., and Van der Beek, P. A.: Present-day uplift of the western Alps,
618 *Sci. Rep.*, 6(1), 1-6, <https://doi.org/10.1038/srep28404>, 2016.

619 Passchier, C.W. and Trouw, R.A.J.: *Microtectonics*, 2nd rev. ed. Springer, Berlin, New York, 2005.

620 Paton, C., Hellstrom, J., Paul, B., Woodhead, J., and Hergt, J.: Iolite: Freeware for the visualisation
621 and processing of mass spectrometric data, *J. Anal. Atom. Spectrom.*, 26(12), 2508-2518,
622 <https://doi/10.1039/c1ja10172b>, 2011.

623 Ring, U. and Gerdes, A.: Kinematics of the Alpenrhein- Bodensee graben system in the Central Alps:
624 Oligocene/Miocene transtension due to formation of the Western Alps arc, *Tectonics*, 35(6), 1367-
625 1391, <https://doi.org/10.1002/2015TC004085>, 2016.

626 Roberts, N.M.W., Rasbury, E.T., Parrish, R.R., Smith, C.J., Horstwood, M.S.A., and Condon, D.J.: A
627 calcite reference material for LA-ICP-MS U-Pb geochronology: Calcite RM for LA-ICP-MS U-Pb
628 dating, *Geochem. Geophys. Geosyst.*, 18, 2807–2814, <https://doi.org/10.1002/2016GC006784>,
629 2017.

630 Roberts, N.M.W., Drost, K., Horstwood, M.S.A., Condon, D.J., Chew, D., Drake, H., Milodowski,
631 A.E., McLean, N.M., Smye, A.J., Walker, R.J., Haslam, R., Hodson, K., Imber, J., and Beaudoin,
632 N.: LA-ICP-MS U-Pb carbonate geochronology: strategies, progress, and application to fracture-
633 fill calcite, *Geochronology*, <https://doi.org/10.5194/gchron-2019-15>, 2020.

634 Rolland, Y., Rossi, M., Cox, S. F., Corsini, M., Mancktelow, N., Pennacchioni, G., Fronari, M., and
635 Boullier, A.M.: ⁴⁰Ar/³⁹Ar dating of synkinematic white mica: insights from fluid-rock reaction in
636 low-grade shear zones (Mont Blanc Massif) and constraints on timing of deformation in the NW
637 external Alps, *Geological Society, London, Special Publications*, 299(1), 293-315,
638 <https://doi.org/10.1144/SP299.18>, 2008.

639 Rolland, Y. and Rossi, M.: Two-stage fluid flow and element transfers in shear zones during collision
640 burial-exhumation cycle: Insights from the Mont Blanc Crystalline Massif (Western Alps), *J.*
641 *Geodyn.*, 101, 88-108, <https://doi.org/10.1016/j.jog.2016.03.016>, 2016.

642 Rossi, M., Rolland, Y., Vidal, O., and Cox, S.F.: Geochemical variations and element transfer during
643 shear-zone development and related episyenites at middle crust depths: insights from the Mont
644 Blanc granite (French-Italian Alps), *Geological Society, London, Special Publications*, 245, 373–
645 396, <https://doi.org/10.1144/GSL.SP.2005.245.01.18>, 2005.

646 Rossi, M. and Rolland, Y.: Stable isotope and Ar/Ar evidence of prolonged multiscale fluid flow
647 during exhumation of orogenic crust: Example from the Mont Blanc and Aar Massifs (NW Alps):
648 Multi-scale fluid flow in the Alps, *Tectonics*, 33, 1681–1709,
649 <https://doi.org/10.1002/2013TC003438>, 2014.

650 Rothé, E.: *La sismicité des Alpes occidentales. Annales de l'Institut de Physique du Globe de*
651 *Strasbourg*, III, 1941.

652 Rubatto, D. and Hermann, J.: Zircon formation during fluid circulation in eclogites (Monviso, Western
653 Alps): implications for Zr and Hf budget in subduction zones, *Geochim. et Cosmochim. Ac.*, 67,
654 2173–2187, [https://doi.org/10.1016/S0016-7037\(02\)01321-2](https://doi.org/10.1016/S0016-7037(02)01321-2), 2003.

655 Salimbeni, S., Zhao, L., Malusà, M., Guillot, S., Pondrelli, S., Margheriti, L., Paul, A., Solarino, S.,
656 Aubert, C., Dumont, T., Schwartz, S., Wang, Q., Xu, X., Zheng, T., and Zhu, R.: Fossil and active
657 mantle flows in the western Alpine region unravelled by seismic anisotropy analysis and high-
658 resolution P wave tomography, *Tectonophysics*, 731-732, 35–47,
659 <https://doi.org/10.1016/j.tecto.2018.03.002>, 2018.

660 Sanchez, G., Rolland, Y., Schneider, J., Corsini, M., Oliot, E., Goncalves, P., Verati, C., Lardeaux, J.-
661 M., and Marquer D.: Dating low-temperature deformation by $^{40}\text{Ar}/^{39}\text{Ar}$ on white mica, insights
662 from the Argentera-Mercantour Massif (SW Alps), *Lithos*, 125(1-2), 521-536,
663 <https://doi.org/10.1016/j.lithos.2011.03.009>, 2011.

664 Seward, D. and Mancktelow, N.S.: Neogene kinematics of the central and western Alps: Evidence
665 from fission-track dating, *Geology*, 22(9), 803-806, [https://doi.org/10.1130/0091-
666 7613\(1994\)022<0803:NKOTCA>2.3.CO;2](https://doi.org/10.1130/0091-7613(1994)022<0803:NKOTCA>2.3.CO;2), 1994.

667 Schmid, S.M. and Kissling, E.: The arc of the western Alps in the light of geophysical data on deep
668 crustal structure, *Tectonics*, 19, 62–85, <https://doi.org/10.1029/1999TC900057>, 2000.

669 Schwartz, S., Lardeaux, J.M., Tricart, P., Guillot, S., and Labrin, E.: Diachronous exhumation of HP-
670 LT metamorphic rocks from south-western Alps: evidence from fission-track analysis, *Terra Nova*,
671 19, 133–140, <https://doi.org/10.1111/j.1365-3121.2006.00728.x>, 2007.

672 Schwartz, S., Gautheron, C., Audin, L., Dumont, T., Nomade, J., Barbarand, J., Pinna-Jamme, R., and
673 van der Beek, P.: Foreland exhumation controlled by crustal thickening in the Western Alps,
674 *Geology*, 45, 139-142, <https://doi.org/10.1130/G38561.1>, 2017.

675 Simon-Labric, T., Rolland, Y., Dumont, T., Heymes, T., Authemayou, C., Corsini, M., and Fornari,
676 M.: $^{40}\text{Ar}/^{39}\text{Ar}$ dating of Penninic Front tectonic displacement (W Alps) during the Lower Oligocene
677 (31-34 Ma), *Terra Nova*, 21, 127–136, <https://doi.org/10.1111/j.1365-3121.2009.00865.x>, 2009.

678 Smeraglia, L., Fabbri, O., Choulet, F., Buatier, M., Boulvais, P., Bernasconi, S.M., and Castorina, F.:
679 Syntectonic fluid flow and deformation mechanisms within the frontal thrust of a foreland fold-
680 and-thrust belt: Example from the Internal Jura, Eastern France, *Tectonophysics*, 778, 228178.
681 <https://doi.org/10.1016/j.tecto.2019.228178>, 2020.

682 Sternai, P., Sue, C., Husson, L., Serpelloni, E., Becker, T.W., Willett, S.D., Faccenna, C., Di Giulio,
683 A., Spada, G., Jolivet, L., Valla, P., Petit, C., Nocquet, J.-M., Walpersdorf, A., and Castellort, S.:
684 Present-day uplift of the European Alps: Evaluating mechanisms and models of their relative
685 contributions, *Earth-Sci. Rev.*, 190, 589–604, <https://doi.org/10.1016/j.earscirev.2019.01.005>,
686 2019.

687 Sue, C. and Tricart, P.: Late Alpine brittle extension above the Frontal Pennine Thrust near Briançon,
688 Western Alps, *Eclogae Geol. Helv.*, 92(2), 171-181, <https://doi.org/10.5169/SEALS-168659>, 1999.

689 Sue, C. and Tricart, P.: Neogene to ongoing normal faulting in the inner western Alps: a major
690 evolution of the alpine tectonics, *Tectonics*, 22, 1–25, <https://doi.org/10.1029/2002TC001426>,
691 2003.

692 Sue, C., Delacou, B., Champagnac, J.-D., Allanic, C., Tricart, P., and Burkhard, M.: Extensional
693 neotectonics around the bend of the Western/Central Alps: an overview, *Int. J. Earth Sci. (Geol*
694 *Rundsch)*, 96, 1101–1129, <https://doi.org/10.1007/s00531-007-0181-3>, 2007.

695 Sue, C., Thouvenot, F., Fréchet, J., and Tricart, P.: Widespread extension in the core of the western
696 Alps revealed by earthquake analysis, *J. Geophys. Res.-Sol. Ea.*, 104(B11), 25611-25622,
697 <https://doi.org/10.1029/1999JB900249>, 1999.

698 Tardy, M., Deville, E., Fudral, S. E. R. E., Guellec, S., Ménard, G., Thouvenot, F., and Vialon, P.:
699 *Interprétation structurale des données du profil de sismique réflexion profonde ECORS-CROP*
700 *Alpes entre le front Pennique et la ligne du Canavese (Alpes occidentales)*, *Mém. S. Géol. F.*, 156,
701 217-226, 1990.

702 Thouvenot, F., Fréchet, J., Pinter, N., Gyula, G., Weber, J., Stein, S., and Medak, D. (Eds.): Seismicity
703 along the northwestern edge of the Adria Microplate, *The Adria Microplate: GPS Geodesy,*
704 *Tectonics and Hazards*, *Nato Si. S. IV Ear. En.* Kluwer Academic Publishers, Dordrecht, 335–349.
705 https://doi.org/10.1007/1-4020-4235-3_23, 2006.

706 Tricart, P.: From passive margin to continental collision; a tectonic scenario for the Western Alps,
707 *Am. J. Sci.*, 284(2), 97-120, <https://doi.org/10.2475/ajs.284.2.97>, 1984.

708 Tricart, P., Schwartz, S., Sue, C., Poupeau, G., and Lardeaux, J.-M.: La dénudation tectonique de la
709 zone ultradauphinoise et l'inversion du front Briançonnais au sud-est du Pelvoux (Alpes
710 occidentales); une dynamique miocène à actuelle, *B. Soc. Geol. Fr.*, 172(1), 49-58,
711 <https://doi.org/10.2113/172.1.49>, 2001.

712 Tricart, P., Lardeaux, J.-M., Schwartz, S., and Sue, C.: The late extension in the inner western Alps: a
713 synthesis along the south-Pelvoux transect, *B. Soc. Geol. Fr.*, 177, 299–310,
714 <https://doi.org/10.2113/gssgfbull.177.6.299>, 2006.

715 Tricart, P., Van Der Beek, P., Schwartz, S., and Labrin, E.: Diachronous late-stage exhumation across
716 the western Alpine arc: constraints from apatite fission-track thermochronology between the
717 Pelvoux and Dora-Maira Massifs, *J. Geol. Soc.*, 164, 163–174, [https://doi.org/10.1144/0016-](https://doi.org/10.1144/0016-76492005-174)
718 [76492005-174](https://doi.org/10.1144/0016-76492005-174), 2007.

719 Vermeesch, P.: IsoplotR: A free and open toolbox for geochronology, *Geosci. Front.*, 9(5), 1479-1493,
720 <https://doi.org/10.1016/j.gsf.2018.04.001>, 2018.

721 Walker, J., Cliff, R.A., and Latham, A.G.: U-Pb isotopic age of the StW 573 hominid from
722 Sterkfontein, South Africa. *Science*, 314(5805), 1592-1594, <https://doi.org/10.1126/science.1132916>,
723 2006.

724 Walpersdorf, A., Pinget, L., Vernant, P., Sue, C., Deprez, A., and the RENAG team.: Does Long-Term
725 GPS in the Western Alps Finally Confirm Earthquake Mechanisms? , *Tectonics*, 37, 3721–3737.
726 <https://doi.org/10.1029/2018TC005054>, 2018.

727 Wells, D. L., and Coppersmith, K. J.: New empirical relationships among magnitude, rupture length,
728 rupture width, rupture area, and surface displacement, *Bull. Seismol. Soc. Am.*, 84(4), 974-1002,
729 1994.

730 Woodhead, J.D. and Hergt, J.M.: Strontium, Neodymium and Lead Isotope Analyses of NIST Glass
731 Certified Reference Materials: SRM 610, 612, 614, *Geostand. Geoanal. Res.*, 25, 261–266,
732 <https://doi.org/10.1111/j.1751-908X.2001.tb00601.x>, 2001.

733 Zhao, L., Paul A., Solarino S., Guillot S., Malusà M., Zheng T., Aubert C., Salimbeni S., Dumont T.,
734 Schwartz S., Pondrelli S., Zhu R., and Wang Q. First seismic evidence for continental subduction
735 beneath the Western Alps, *Geology*, 43, 815-818, <https://doi.org/10.1130/G36833.1>, 2015.